Sedimentary Geology 233 (2011) 129–149

Contents lists available at ScienceDirect

Sedimentary Geology

journal homepage: www.elsevier.com/locate/sedgeo

An extensive erosion surface of a strongly deformed limestone bed in the Gushan and Chaomidian formations (late Middle Cambrian to Furongian), Shandong Province, China: Sequence–stratigraphic implications

Jitao Chen [a,b], S.K. Chough [a,*], Zuozhen Han [b], Jeong-Hyun Lee [a]

[a] School of Earth and Environmental Sciences, Seoul National University, Seoul 151-747, South Korea
[b] College of Geological Science and Engineering, Shandong University of Science and Technology, Qingdao 266510, China

ARTICLE INFO

Article history:
Received 4 September 2010
Received in revised form 3 November 2010
Accepted 5 November 2010
Available online 12 November 2010

Editor: B. Jones

Keywords:
Erosion surface
Soft-sediment deformation
Carbon isotope
Subaerial unconformity
Furongian
North China Platform

ABSTRACT

In order to understand sequence development and sea-level fluctuations during the late Middle Cambrian to early Furongian on the North China epeiric platform, the present study focuses on a unique, subtle erosion surface of an extensive (approx. 100 km), strongly deformed limestone bed in the uppermost part of the Gushan Formation, Shandong Province, China. The Gushan Formation and the overlying Chaomidian Formation consist mainly of shales and a variety of carbonates that were deposited in subtidal environments (e.g., deep subtidal, shallow subtidal, shoreface/shoal, subtidal microbial flat, and restricted platform interior). Three third-order depositional sequences (S1–3) are identified, each of which comprises a thin transgressive systems tract (TST) and a relatively thick highstand systems tract (HST). Each sequence is bounded by a drowning unconformity (SB1), a subaerial unconformity (SB2), or a surface of submarine erosion (SB3). The upper sequence boundary (SB2) of sequence 1 (S1) is represented by a subtle erosion surface of an extensive, deformed limestone bed with a wide variety of soft-sediment deformation structures (e.g., lime mudstone breccias, chaotic wacke-packstone laminae and fragments, homogenized oolites, and clastic dykes), and is overlain by small sporadic microbial buildups and an extensive bioclastic grainstone bed. The deformed limestone was formed during early diagenesis by differential deformation processes (brecciation, liquefaction/fluidization, and injection) which were most likely induced by pore-water overpressure during the period of rapid sea-level fall. Despite the lack of subaerial exposure features (e.g., paleokarst, paleosol, etc.), the characteristics of the erosion surface (cutting well-lithified sediment below), the missing of a significant geological record (the *Prochuangia* biozone), and the worldwide correlatable positive carbon isotope excursion collectively indicate that the erosion surface developed under conditions of subaerial exposure after contemporaneous marine cementation of the deformed sediment. The missing of the *Prochuangia* biozone is most likely due to non-deposition at a subaerial hiatal surface. The erosion surface was submerged as a result of subsequent rise in sea level, where sporadic microbial buildups formed under suitable conditions. Freshly deposited, winnowed, shell-dominated transgressive lag deposits (containing *Chuangia* trilobite fragments, brachiopod shells, and abundant glauconite grains) formed with continued rise in sea level, which became, in turn, overlain by shale-dominated facies. The unique combination of the subtle erosion surface (*sensu stricto* a subaerial unconformity) and the underlying deformed limestone bed provides an important criterion for recognizing the subtle changes in relative sea level on shallow epeiric platforms.

1. Introduction

Depositional sequences formed during high-order (third- and higher-order) sea-level changes of greenhouse periods are commonly devoid of distinct features for prolonged subaerial exposure such as paleokarst, paleosol, and cement fabrics (Read and Goldhammer, 1988; Lehrmann and Goldhammer, 1999). They are often bounded by either turnaround surfaces of progradational to retrogradational stacking patterns of parasequences (Lehrmann and Goldhammer, 1999; Kwon et al., 2006) or drowning unconformities represented by an abrupt shallowing to deepening facies shift (Schlager, 1999; Kolata et al., 2001). High-order depositional sequences can also be identified by shallowing-upward successions bounded by surfaces of marine flooding or submarine erosion (Osleger and Montañez, 1996; Meng et al., 1997; Hamon and Merzeraud, 2008). On the other hand, subaerial exposure surfaces may develop as sequence boundaries in epeiric platforms as a result of emersion of sediment due to progradation processes and sea-level fluctuations (Tucker and Wright, 1990;

* Corresponding author. Tel.: +82 2 886 1423.
E-mail addresses: jitaochen@126.com (J. Chen), sedlab@snu.ac.kr (S.K. Chough).

0037-0738/$ – see front matter © 2010 Elsevier B.V. All rights reserved.
doi:10.1016/j.sedgeo.2010.11.002

Wright, 1994; Holland and Patzkowsky, 1998). They are, however, not readily recognized due to either lateral discontinuity (e.g., Vanstone, 1998) or removal by subsequent submarine erosion (e.g., Rasmussen and Neumann, 1988; Driese et al., 1994; Holland and Patzkowsky, 1998).

A thick Cambrian–Ordovician succession (approx. 1800 m) of mixed siliciclastic and carbonate rocks was deposited on the North China Platform (Figs. 1 and 2). According to Meng et al. (1997), the entire succession represents a second-order transgression and regression with high-order fluctuations of the sea level. The late Middle Cambrian to Furongian succession (Gushan and Chaomidian formations) consists mainly of shales and subtidal carbonate facies, which contains a number of deformed beds, exclusively in the form of a variety of limestone breccias and conglomerates (Chen et al., 2009a). Among them, a laterally extensive (approx. 100 km), strongly deformed limestone bed with complex soft-sediment deformation structures occurs in the uppermost part of the Gushan Formation. The deformed limestone bed is truncated with a low-relief, irregular erosion surface which is overlain by a bioclastic grainstone bed of the Chaomidian Formation. The primary objective of the present study is to illustrate the formative processes of the erosion surface based on detailed sedimentary facies. It warrants a detailed investigation for a new sequence boundary, because both the deformed limestone bed and its erosion surface conceal the history of relative sea-level changes.

2. Geological setting

The Sino-Korean Block, a stable craton in the tropical to subtropical zone during the Cambrian (e.g., Scotese and McKerrow, 1990), is bounded to the north by a major suture zone, the Hinggan fold belt (Meyerhoff et al., 1991). The Qinling–Dabieshan fold belt demarcates the southern margin of the block against the South China Block (Fig. 1). A major offset (approx. 300 km) of the sinistral strike–slip fault, the Tan–Lu fault, occurs in the eastern part of the Sino-Korean Block, formed by the collision of the South China Block against the Sino-Korean Block during the Early Triassic (Chough et al., 2000) (Fig. 1A).

The North China Platform, formed in a vast area (1,500,000 km^2) of the Sino-Korean Block, comprises a thick (approx. 1800 m) Cambrian–Ordovician succession of mixed carbonate and siliciclastic sediments (Meng et al., 1997). The Cambrian succession in Shandong Province, China comprises six lithostratigraphic units (the Liguan, Zhushadong, Mantou, Zhangxia, Gushan, and Chaomidian formations in ascending order), unconformably overlying Precambrian granitic gneiss or locally Late Proterozoic metasedimentary rocks, and conformably underlying Ordovician dolostones (Sanshanzi Formation) (Chough et al., 2010) (Fig. 2).

The Cambrian strata in Shandong Province are superbly exposed and have long been regarded as type sections for stratigraphic units of the North China Platform (Meyerhoff et al., 1991); they yield abundant and diverse fossils such as trilobites, gastropods, brachiopods, and cephalopods. In the Cambrian succession, twenty-one trilobite biozones have been identified (Chough et al., 2010) (Fig. 2). The Gushan Formation accumulated during the Kushanian Stage (*Blackwelderia* and *Neodrepanura*), whereas the Chaomidian Formation deposited during the Changshanian Stage (*Chuangia*, *Changshania–Irvingella*, and *Kaolishania*) and the Fengshanian Stage (*Ptychaspis–Tsinania*, *Quadraticephalus*, and *Mictosaukia*) (Fig. 2). The *Prochuangia* biozone (in between the *Neodrepanura* and *Chuangia* biozones) is absent in the late Middle Cambrian to Furongian succession in Shandong Province, although it occurs in Liaoning Province (NE China) and the Taebaeksan Basin (South Korea) (Park et al., 2007) (Figs. 1A and 2).

3. Materials and methods

The present study is based on a detailed description of sedimentary facies (at a 1:10 or 1:50 scale; approx. 800 m in thickness) of four major outcrop sections (the Tangwangzhai, Laopozhuang, Wanliangyu, and Jiulongshan sections) of the Gushan and Chaomidian formations in Shandong Province, China (Fig. 1B). The deformed limestone bed was correlated by tracking the outcrop sections for over 100 km. Line drawings were made in the field and laboratory to portray in detail the sedimentary structures (soft-sediment deformation structures, erosion surfaces, etc.). Sampled specimens were cut and polished for slabs and

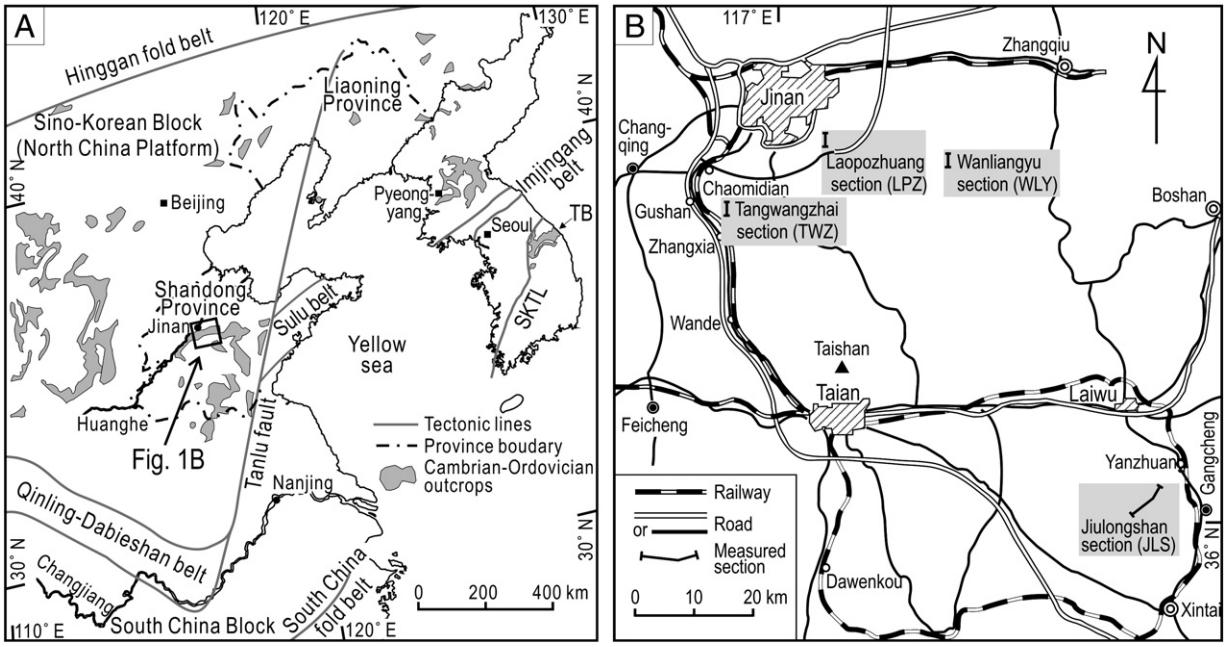

Fig. 1. A. Major tectonic boundaries of the North China Platform and distribution of the Cambrian–Ordovician outcrops (modified after Kwon et al., 2006). SKTL: South Korean Tectonic Line, TB: Taebaeksan Basin. B. Location map of measured sections of the Gushan and Chaomidian formations (late Middle Cambrian to Furongian) in Shandong Province, China.

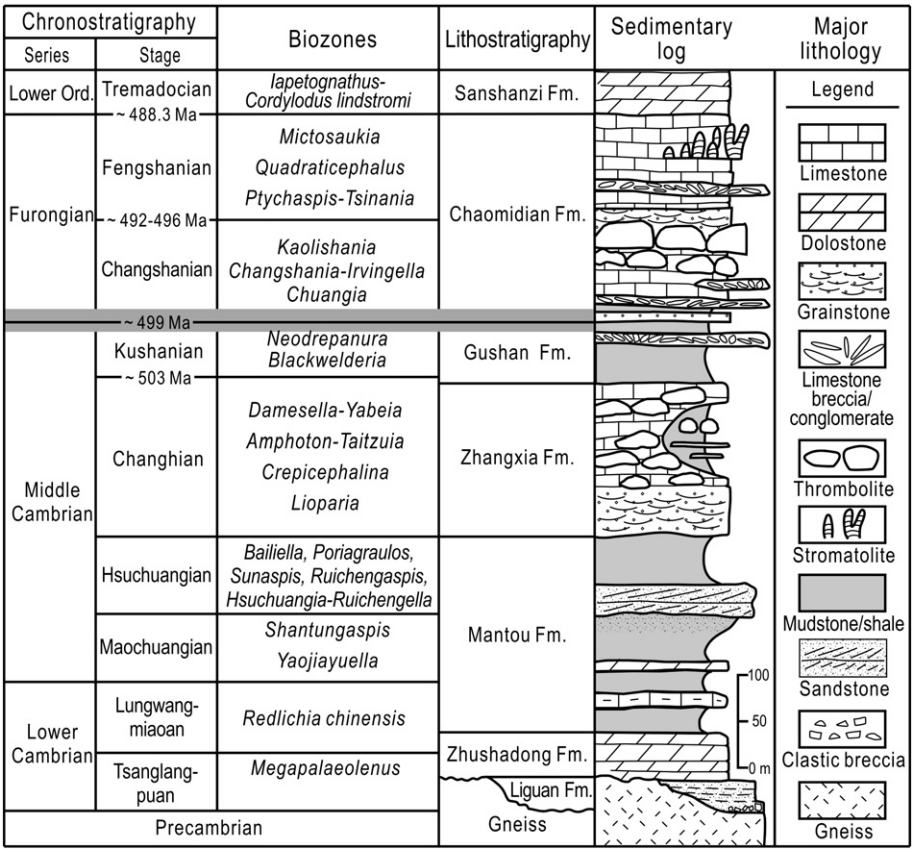

Fig. 2. Schematic stratigraphy of the Cambrian succession in Shandong Province, China. The shaded interval indicates the stratigraphic position of the extensive deformed limestone bed and the absence of the *Prochuangia* biozone.

thin sections for microscopic observation of lithofacies, especially those of the deformed limestone and its overlying microbialites and grainstones. Samples for carbon isotopic analysis were collected by drilling 2–10 mg from the fresh surface of homogeneous micritic limestone beds or clasts in every 10–20 cm interval in the Wanliangyu section. Analytical work was carried out by standard procedures in the stable isotope laboratory at Nanjing Normal University (China).

4. Sedimentary facies and sequence–stratigraphic framework

4.1. Sedimentary facies and facies associations

The Gushan Formation and the overlying Chaomidian Formation consist mainly of shales and various types of carbonate beds that can be divided into 15 sedimentary facies in terms of lithology (grain size and composition) and sedimentary structures (Table 1). According to the assembly of sedimentary facies, five facies associations (FA1–5) can be established in the Gushan and Chaomidian formations (Table 2). These facies associations are well correlated among the measured sections (Fig. 3). In order to provide a sequence–stratigraphic framework, each association is described and interpreted as for their depositional environments and sequences.

4.1.1. FA1: shale-dominated facies association

Description: FA1 is dominated by greenish-gray (yellowish-gray) shale (facies Sh), frequently intercalated with thin homogeneous lime mudstone beds, forming limestone/shale alternations (facies L–S) (Fig. 4A). The limestone/shale alternations were commonly transformed into limestone breccias (facies Cp) during early diagenesis. FA1 partly consists of decimeter- to meter-scale cycles that comprise facies L–S in the lower part and facies Sh in the upper part (Fig. 4B). A few calcarenite (facies CA) beds with normal grading and small-scale load and flame structures occur (Fig. 4C).

Interpretation: FA1 is overall representative of a low-energy, deep-water environmental setting (e.g., deep subtidal) (Markello and Read, 1981; Glumac and Walker, 2000; Elrick and Snider, 2002). Shale was most likely deposited by suspension settling of argillaceous airborne material (cf. Dalrymple et al., 1985), whereas the limestone/shale alternations were formed by the frequent input of carbonates during background sedimentation of clay (Elrick and Snider, 2002). The calcarenite beds with a sharp lower boundary were deposited by dilute density (turbidity) currents originated on the local slopes (cf. Drzewiecki and Simó, 2002; Payros and Pujalte, 2008; Woo, 2009).

4.1.2. FA2: thin-bedded limestone facies association

Description: FA2 comprises primarily thin-bedded limestone facies, with a predominance of limestone/shale alternations, limestone/marlstone alternations, and thin-bedded lime mudstones (facies L–S, L–M, and Ltb) in the lower part, and low-angle or ripple cross-laminated calcisiltites, planar and trough cross-stratified grainstones, and stratified conglomerates (facies Cl, Gptc, and Cs) in the upper part (Table 2; Fig. 5). Facies L–S and L–M gradually change into Ltb, which is overlain by a gravelly grainstone and a cross-stratified conglomerate (facies Gg and Cs) with an irregular, sharp boundary (Fig. 5B). A few biohermal to biostromal microbialites (facies Mb) partly occur (Fig. 5A).

Interpretation: The thin-bedded limestones intercalated with shales (marlstones) (facies L–S, L–M, and Ltb) were formed by the frequent input of carbonate sediments during background sedimentation of siliciclastic fines. The laminated calcisiltites, the planar and trough cross-stratified grainstones, and the conglomerates (facies Cl,

Table 1
Sedimentary facies in the Gushan and Chaomidian formations.

Sedimentary facies	Description	Interpretation
Shale (facies Sh)	Greenish-gray (yellowish-gray and partly dark purple) shale; mainly composed of quartz and clay minerals, and some calcite and dolomite; intercalated with calcareous nodules or irregular concretions; usually fissile and papery, partly calcareous.	Low-energy subtidal deposits most likely below storm-wave base (Markello and Read, 1981; Osleger and Read, 1991).
Limestone/shale alternation (facies L–S)	Alternation of planar to nodular limestone and greenish-gray shale; limestone composed of micrite; shale composed mainly of argillaceous materials (quartz and clay minerals, 81%), and small fractions of calcite and dolomite (19%); sporadic horizontal burrows; well-preserved trilobite fossils (e.g., *Blackwelderia* and *Neodrepanura*) on bedding plane.	Low-energy subtidal deposit below fair-weather wave base (Woo, 1999; Kwon et al., 2002; Kwon and Chough, 2005).
Limestone/marlstone alternation (facies L–M)	Alternation of limestone and marlstone layers; about 1 cm in thickness; limestone composed of micrite with trilobite fragments (5–20%); marlstone composed of dolomite (16.11%), calcite (53.93%), and argillaceous materials (29.96%); slightly bioturbated with sporadic horizontal or inclined burrows; lenses of bioclasts intercalated in some horizons.	Low-energy subtidal deposit below fair-weather wave base (Pfeil and Read, 1980; Moshier, 1986; Calvet and Tucker, 1988; Keller, 1997).
Thin-bedded lime mudstone (facies Ltb)	Slightly bioturbated thin-bedded lime mudstone; lime mudstone composed of micrite and small fractions of bioclasts; sporadic horizontal to inclined burrows; commonly overlying L–S or L–M with gradational boundary, forming decimeter- to meter-scale units.	Low-energy subtidal deposit modified by bioturbation (Calvet and Tucker, 1988).
Laminated calcisiltite (facies Cl)	Parallel, ripple, and low-angle cross-laminated calcisiltite intercalated with dolomitic marlstone or shale; composed of silt-sized calcite particles; wavy-bedded, unidirectional and low-angle cross-lamination with internal truncational boundary; climbing ripples; partly bioturbated with burrows cutting laminae.	Subtidal deposits by unidirectional currents (partly combined with oscillatory movement of water) induced by storms (Woo and Chough, 2007).
Bioturbated wackestone (facies Wb)	Moderately to severely bioturbated (ichnofossil index −3 and −4); horizontal to inclined burrows; mottled texture; composed mainly of micrite, fossil fragments, and peloids; partly intercalated with thin bioclastic grainstone with sharp lower boundary.	Low-energy subtidal deposits modified by bioturbation (Osleger and Montañez, 1996; Sanders and Höfling, 2000).
Wackestone to grainstone (facies W–G)	Flaser-bedded wackestone separated by shale partings; slightly bioturbated; often intercalated with lenses or thin layers of grainstone with sharp lower boundary; grainstone commonly massive, normally graded, or planar and cross-stratified; abundant and variable fossil fragments such as cephalopods, bivalves, gastropods, trilobites, algae, and echinoderms.	Relatively low-energy subtidal deposits with intermittent higher energy deposits (Rees et al., 1976; Nakazawa et al., 2009).
Hummocky and swaley cross-stratified grainstone (facies Ghsc)	Peloidal grainstone, composed of coarse silt- to very fine sand-size peloids and small fraction of fossil fragments; hummocky cross-stratified bed is either laterally continuous or discontinuous, varying in thickness from a few dm to 2 m; thick beds amalgamated with internal sharp boundaries; *Skolithos*, 1–5 cm in depth; variation in thickness of laminae.	Storm-induced combined flows (Allen, 1985; Arnott and Southard 1990; Myrow and Southard, 1996; Molgat and Arnott, 2001; Myrow et al., 2004).
Planar and trough cross-stratified grainstone (facies Gptc)	Cross-stratified grainstone with planar to tangential contact to the base; partly trough cross-stratified; undulatory bedforms; composed of fossil fragments (trilobites, brachiopods, echinoderms, and algae), ooids, and glauconite grains.	Subaqueous 2D or 3D dune (Strasser, 1986; Moshier, 1986; Betzler et al., 2007; Palma et al., 2007).
Gravelly grainstone (facies Gg)	Massive or normally graded gravelly packstone to grainstone; composed of bioclasts (trilobites, brachiopods, algae, echinoderms, and cephalopods; a few mm up to 10 mm in length) and peloids (0.2–0.5 mm in diameter); subangular granules and pebbles of lime mudstone to grainstone commonly at base.	Moderately agitated shallow-subtidal deposits (Glumac and Walker, 2000; Woo and Chough, 2007).
Calcarenite (facies CA)	Calcarenite containing a few clasts of lime mudstone; composed of packstone to grainstone with elongate trilobite fragments; crudely laminated or normally graded; overlying lime mudstone with irregular sharp boundaries, showing load and flame structures.	Deposition from dilute density (turbidity) currents (Drzewiecki and Simó, 2002; Payros and Pujalte, 2008; Woo, 2009).
Stratified limestone conglomerate (facies Cs)	Polymictic limestone clasts in bioclastic and peloidal grainstone matrix; subrounded to rounded clasts; horizontal- to cross-stratified; partly imbricated clasts; clast- or matrix supported; conglomerate beds amalgamated with internal truncation; sharp irregular lower boundary and gradational upper boundary to facies Ghsc or Gptc.	Deposits by strong currents or waves induced by storms (Walker and Plint, 1992; Demicco and Hardie, 1994).
Limestone breccia (facies Cp)	Monomictic to oligomictic clasts in a matrix of marlstone and/or grainstone; flat to irregular, sheet-, disc-, or blade-shaped clasts; random clast positions (intact, inclined, vertical, and disorganized); transitional boundaries from underlying bed; laterally discontinuous.	Sediment deformation during early diagenesis (Chough et al., 2001; Kwon et al., 2002; Chen et al., 2009a).
Biostromal microbialite (facies Mb)	Characterized by biostromal microbialites of various macrostructures (e.g., maceriate and columnar structures); composed of micrite, peloids, ooids, fragments of fossils (trilobites, algae, and brachiopods), and cement of sparry calcite as well as calcified *Girvanella* and *Renalcis* colonies.	Subtidal deposits near fair-weather wave base (Moshier, 1986; Adams and Grotzinger, 1996; Glumac and Walker, 2000).
Columnar stromatolite facies (facies Sc)	Centimeter- to meter-scale columnar-shaped; bioclastic grainstone and bioturbated wackestone between columns; composed of micritic *Girvanella* colonies, peloids, fragments of fossils (trilobites, algae, cephalopods, and gastropods), and partly intraclasts.	High-energy subtidal deposits with occasional lower-energy deposits (Garrett et al., 1970; Rees et al., 1976; Dravis, 1983).

Gptc, and Cs) reflect the activity of waves and/or currents. The microbialites were deposited under suitable conditions regarding depth, light, temperature, and turbidity (James and Bourque, 1992; Saltzman, 1999). The occurrence of both abundant carbonate deposits and wave- and current-induced structures suggests that FA2 was formed in relatively shallow environments (e.g., shallow subtidal) (cf. Burchette and Wright, 1992; Kwon et al., 2006).

4.1.3. FA3: grainstone facies association

Description: FA3 occurs in the lowermost and middle parts of the Chaomidian Formation (Fig. 3) and is dominated by various grainstone facies with fragmentary bioclasts, ooids, peloids, intraclasts, and abundant glauconite grains (Table 2; Fig. 6A–F). The FA3 of the middle part of the Chaomidian Formation starts with either a gravelly grainstone (facies Gg) or a planar and trough cross-stratified

Table 2
Constituent facies and interpretations of facies associations.

Facies association (FA)	Major constituent facies	Depositional environments
FA1: shale-dominated facies association	Shale (Sh), limestone/shale alternation (L–S), limestone breccia (Cp), calcarenite (CA)	Deep subtidal
FA2: thin-bedded limestone facies association	Limestone/shale alternation (L–S), limestone/marlstone alternation (L–M), thin-bedded lime mudstone (Ltb), laminated calcisiltite (Cl), limestone breccia (Cp), cross-stratified lime conglomerate (Cs)	Shallow subtidal
FA3: grainstone facies association	Planar and trough cross-stratified grainstone (Gptc), hummocky and swaley cross-stratified grainstone (Ghsc), gravelly grainstone (Gg), cross-stratified conglomerate (Cs)	Shoreface/shoal
FA4: microbialite facies association	Biostromal microbialite (Mb), planar and trough cross-stratified grainstone (Gptc), gravelly grainstone (Gg)	Subtidal microbial flat
FA5: bioturbated wackestone to grainstone facies association	Bioturbated wackestone (Wb), wackestone to grainstone (W-G), gravelly grainstone (Gg), columnar stromatolite (Sc), planar and trough cross-stratified grainstone (Gptc), limestone/shale alternation (L–S)	Restricted platform interior

grainstone (facies Gptc), and alternates upward with hummocky and swaley cross-stratified grainstones (facies Ghsc) (Fig. 6). Cross-stratified conglomerates, laminated calcisiltites, and limestone/shale alternations (facies Cs, Cl, and L–S) are rarely intercalated with facies Gptc and Ghsc (Fig. 3).

Interpretation: FA3 was formed near the normal wave base in a shallow-water, high-energy setting. Facies Gptc and Gg are indicative of frequent reworking by currents and waves above the normal wave base (e.g., shoal) (Betzler et al., 2007; Palma et al., 2007), whereas facies Ghsc is typical of deposits reworked by storm-induced combined flows below the normal wave base (e.g., mid-ramp or shoreface) (cf. Burchette and Wright, 1992; Myrow et al., 2004). The upward change from facies Gptc to Ghsc reflects deepening of the water. Facies Cl and L–S were probably formed in depressions among dunes or hummocks under fair-weather conditions.

4.1.4. FA4: microbialite facies association

Description: FA4 is dominated by a thick-bedded (up to 3 m thick) biostromal microbialite (facies Mb) with various macrostructures, changing from maceriate to columnar structures upward (Lee et al., 2010) (Fig. 6A, B). The microbialite beds (up to 10 m in thickness) are either interrupted by sharp internal boundaries in the Tangwangzhai and Laopozhuang sections, or intercalated with cross-stratified limestone conglomerates, hummocky and swaley cross-stratified grainstones, and gravelly grainstones (facies Cs, Ghsc, and Gg) in the Jiulongshan section. FA4 is overlain by various types of grainstones of FA3 with an irregular, sharp boundary (Figs. 3 and 6).

Interpretation: The widely distributed thick microbial buildups might have formed an extensive subtidal microbial flat under optimum conditions of water depth, sunlight, temperature, nutrient availability, and salinity (Saltzman, 1999). The upward change in macrostructures from maceriae to columns and the incorporated coarse grains suggest a shallowing water depth and a high-energy setting (Grotzinger, 1986; James and Bourque, 1992; Lee et al., 2010). The microbial buildups were scoured by strong currents and waves, and terminated by a rapid rise in sea level and excessive input of coarse-grained sediments (Adams et al., 2005).

4.1.5. FA5: bioturbated wackestone to grainstone facies association

Description: FA5 is characterized by a thick monotonous succession of mainly bioturbated lime mudstones to wackestones and wackestones to grainstones (facies Wb and W-G) (Table 2; Fig. 7). Thin layers (up to a few dm in thickness) of massive, normally graded, or stratified grainstone and limestone conglomerate, and limestone/shale alternations (facies Gg, Gptc, Cs, and L–S) are commonly interbedded with facies Wb and W–G. Abundant and variable fossil fragments and sporadic cm-scale microbial buildups occur (Fig. 7D). A thick (up to 11 m thick) interval of low-relief columnar stromatolites (facies Sc) is present in the Jiulongshan section (Figs. 3 and 7E).

Interpretation: FA5 is representative of a generally low-energy restricted platform interior (or a wide, shallow lagoon) with intermittent high-energy conditions (cf. Osleger and Montañez, 1996; Nakazawa et al., 2009). The presence of abundant lime mudstones and extensive bioturbation (facies Wb, W–G, and L–S) is suggestive of deposition under low-energy conditions, probably protected from constant reworking by waves and currents due to friction with the low-gradient sea floor, and/or a topographic barrier (carbonate shoals) and microbial buildups (cf. Srinivasan and Walker, 1993). The frequently intercalated grainstone and conglomerate layers were most likely deposited by storm-induced currents which swept sediments from basinward barriers (Elrick and Snider, 2002). The variable fossil composition is suggestive of a subtidal environment with moderate water circulation, which was suitable for various organisms (Chen and Teichert, 1983; Nakazawa et al., 2009).

4.2. Depositional sequences

According to the vertical arrangement of the facies associations, the succession can be grouped into 3 third-order (1–10 m.y. in duration) depositional sequences (S1–3) bounded by a drowning unconformity (SB1), a subaerial unconformity (SB2), or a surface of submarine erosion (SB3) (Fig. 3). The sequences generally comprise a deepening-upward transgressive systems tract (TST) and a shallowing-upward highstand systems tract (HST) (Fig. 3).

4.2.1. Sequence 1 (S1)

S1 starts at the base of the Gushan Formation, bounded by a drowning unconformity (type-3 sequence boundary) that is characterized by an abrupt change in lithology from the underlying carbonate deposits in the Zhangxia Formation to the overlying shale (FA1) in the lower part of the Gushan Formation (cf. Schlager, 1999) (Fig. 3). The upper part of the sequence contains more carbonates (FA2), reflecting progressive shallowing, most likely due to successive catch-up and progradation during a highstand in sea level. The upper boundary (SB2) of S1 is represented by a unique erosion surface (i.e., a subaerial unconformity) that cuts an extensive, strongly deformed limestone bed with several soft-sediment deformation structures (detailed in Sections 5 and 6).

4.2.2. Sequence 2 (S2)

Bounded by an erosion surface of an extensive, deformed limestone bed, S2 starts with a transgressive systems tract (TST) containing a thin transgressive lag deposit with abundant fossil fragments and glauconite grains (FA3), and a deepening-upward shale-dominated deposit (FA1). A relatively thick coarsening-upward unit containing a thin-bedded limestone facies association (FA2) and a microbialite facies association (FA4) was deposited during a highstand in relative sea level. The thick microbialite bed was terminated by a rise in relative sea level, and became scoured by the subsequent transgressive ravinement, forming the upper sequence boundary (SB3) of S2.

4.2.3. Sequence 3 (S3)

With the subsequent rise in relative sea level, carbonate factories were established under shallow-water conditions; carbonate accumulation kept pace with an increase in accommodation space during

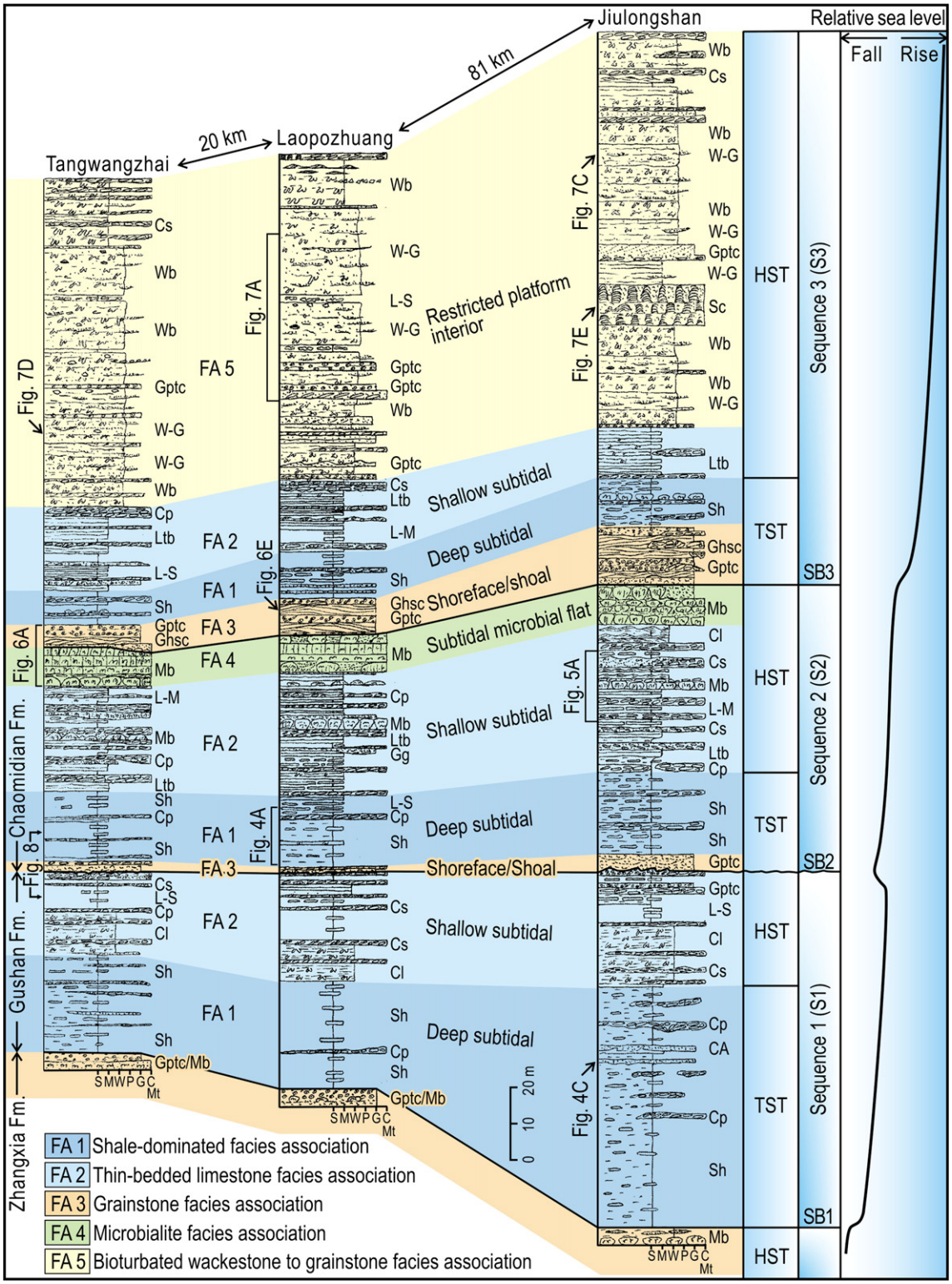

Fig. 3. Facies associations and depositional sequences of three major sections (for section location, see Fig. 1B). S: shale, M: lime mudstone, W: wackestone, P: packstone, G: grainstone, C: limestone conglomerate, Mt: microbialite. Sh: shale, L–S: limestone/shale alternation, L–M: limestone/marlstone alternation, Ltb: thin-bedded lime mudstone, Cl: laminated calcisiltite, Wb: bioturbated wackestone, W–G: wackestone to grainstone, Ghsc: hummocky and swaley cross-stratified grainstone, Gptc: planar and trough cross-stratified grainstone, Gg: gravelly grainstone, CA: calcarenite, Cs: stratified limestone conglomerate, Cp: limestone breccia, Mb: biostromal microbialite, Sc: columnar stromatolite. HST: highstand systems tract, TST: transgressive systems tract. SB: sequence boundary.

the early transgression, resulting in a grainstone facies association (FA3) of S3. The generally deepening-upward grainstone unit (e.g., planar and trough cross-stratified grainstones and hummocky and swaley cross-stratified grainstones) was, in turn, overlain by a thin unit of shale-dominated facies association (FA1), indicating that the carbonate factories were drowned again during the subsequent transgression. A relatively thin, shallow-subtidal deposit (FA2) and a thick unit of restricted platform interior deposits (FA5) progressed during the highstand in sea level. Deposition of S3 was continuous from the Chaomidian Formation to the Sanshanzi Formation (Early

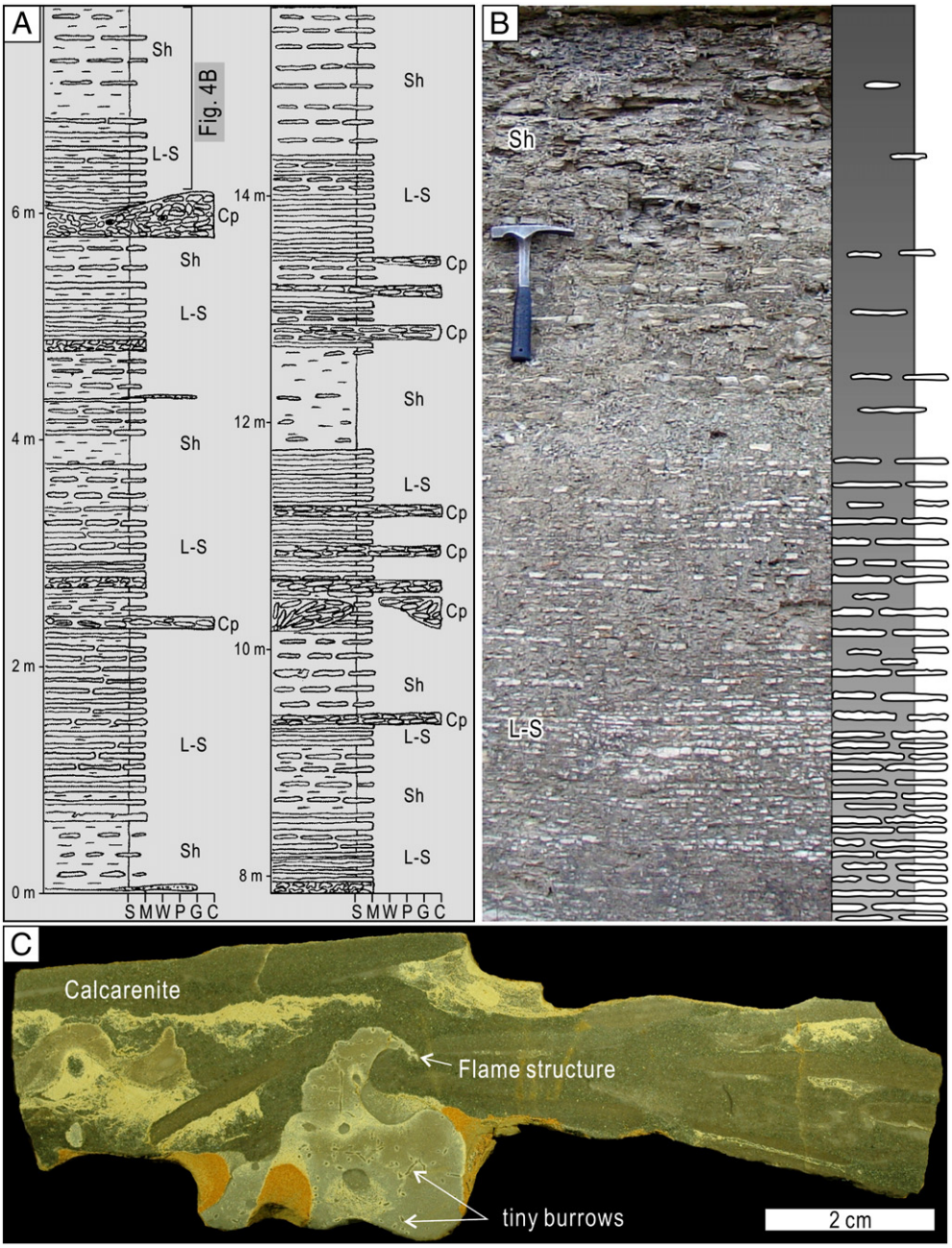

Fig. 4. Shale-dominated facies association (FA1). A. A sedimentary log of FA1 in the lower part of the Chaomidian Formation (Laopozhuang section) (for location, see Fig. 3). S: shale, M: lime mudstone, W: wackestone, P: packstone, G: grainstone, and C: limestone conglomerate. B. An upward gradual change from limestone/shale alternation (facies L–S) to shale (facies Sh). Hammer for scale is 28 cm in length. C. Etched slab of thin calcarenite bed and underlying lime mudstone bed with flame structures in the Jiulongshan section (for location, see Fig. 3).

Ordovician) that consists of dolomitized tidal-flat deposits (Meng et al., 1997). S3 was bounded by the Huaiyuan hiatus in the North China Platform as a result of eustatic sea-level fall during the Early Ordovician (Meng et al., 1997; Kwon et al., 2006).

5. Extensive, strongly deformed limestone bed

5.1. Unique occurrence

The Gushan and Chaomidian formations consist of various ribbon rocks (limestone–shale/marlstone alternations, thin-bedded lime mudstones, and calcisiltites) and other carbonates (e.g., wacke- to grainstones) (Table 1) that contain a variety of soft-sediment deformation structures, exclusively in the form of limestone breccias (conglomerates) and escape structures (Chen et al., 2009a,b). These deformed beds cannot be correlated bed-by-bed among the various outcrops; some are laterally discontinuous and extend for only meters or tens of meters. However, a laterally extensive, strongly deformed limestone bed occurs in the uppermost part of the Gushan Formation in all measured outcrop sections (Tangwangzhai, Laopozhuang, Wanliangyu, and Jiulongshan) (Figs. 3 and 8). It is laterally continuous for about 100 km, with a slight variation in thickness (40–105 cm thick).

The deformed limestone bed (containing *Neodrepanura* trilobite biozone) consists mainly of (deformed) thin-bedded lime mudstones, oolitic and bioclastic wackestones to grainstones, and stratified limestone conglomerates (facies Ltb, Gptc, and Cs) (Table 1; Fig. 8). It comprises various types of soft-sediment deformation structures such as lime mudstone breccias, chaotic wacke-packstone laminae

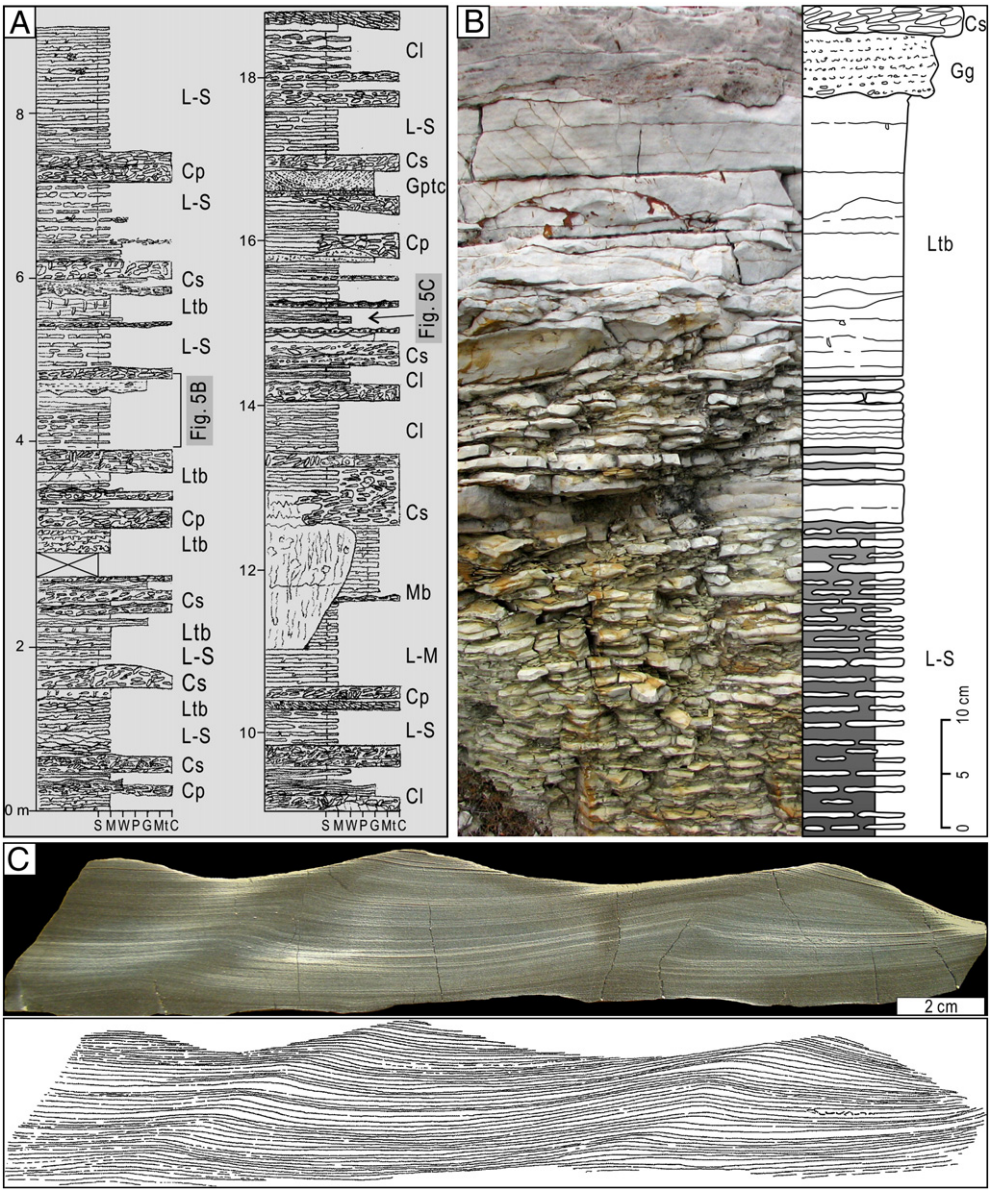

Fig. 5. Thin-bedded limestone facies association (FA2). A. A sedimentary log of FA2 in the lower part of the Chaomidian Formation (Jiulongshan section) (for location, see Fig. 3). S: shale, M: lime mudstone, W: wackestone, P: packstone, G: grainstone, C: limestone conglomerate, and Mt: microbialite. B. A gradual change from limestone/shale alternation (facies L–S) to thin-bedded lime mudstone (facies Ltb), overlain by gravelly grainstone and stratified limestone conglomerate (facies Gg and Cs) with an irregular, sharp boundary. C. Etched slab of climbing-ripple cross-laminated calcisiltite (facies Cl).

and fragments, homogenized (massive) oolites, and clastic dykes (Table 3; Fig. 9). The deformed bed is underlain by the upper part of FA2 in the Gushan Formation which consists mainly of limestone/shale alternations, limestone breccias, and planar and trough cross-stratified oolitic grainstones (facies L–S, Cp, and Gptc) (Figs. 3 and 8). It is truncated by an irregular erosional surface, which is overlain by an extensive bioclastic grainstone bed (containing *Chuangia* biozone). The *Chuangia*-bearing grainstone is, in turn, overlain by shale-dominated facies (FA1) which yield the *Changshania–Irvingella* biozone (Fig. 8). The deformed limestone bed is, therefore, unique for its combination of lateral continuity, complex deformation structures, erosion surface that truncates the bed, and extensive deposition of the overlying *Chuangia*-bearing grainstones.

5.2. Deformation structures and processes

The deformed limestone bed contains a variety of soft-sediment deformation structures. These deformation structures are classified and described here mainly according to the constituent lithology (composition and grain size) and the features of the deformation structures (e.g., lime mudstone breccias, chaotic wacke-packstone laminae and fragments, homogenized oolites, and clastic dykes) (Table 3; Figs. 9–13).

5.2.1. Lime mudstone breccia

Description: The lime mudstone breccia consists mainly of monomictic to oligomictic pebble- to cobble-size clasts of lime mudstone, with a matrix of oolitic grainstone, dolomitic marlstone, or bioclastic wackestone to packstone (Figs. 11 and 12A, B). The clasts are commonly flat or bent, and disc- and blade-shaped with subrounded to angular corners. The lime mudstone breccia occurs usually in the middle and lower parts of the deformed bed (Figs. 10 and 11), showing an ample variation in position of clasts from *in situ* with intrastratal cracks (horizontal) (Fig. 12A) to slightly displaced or dislocated (subhorizontal and inclined) (Fig. 11). The thin limestone beds partly show progressive fragmentation and brecciation

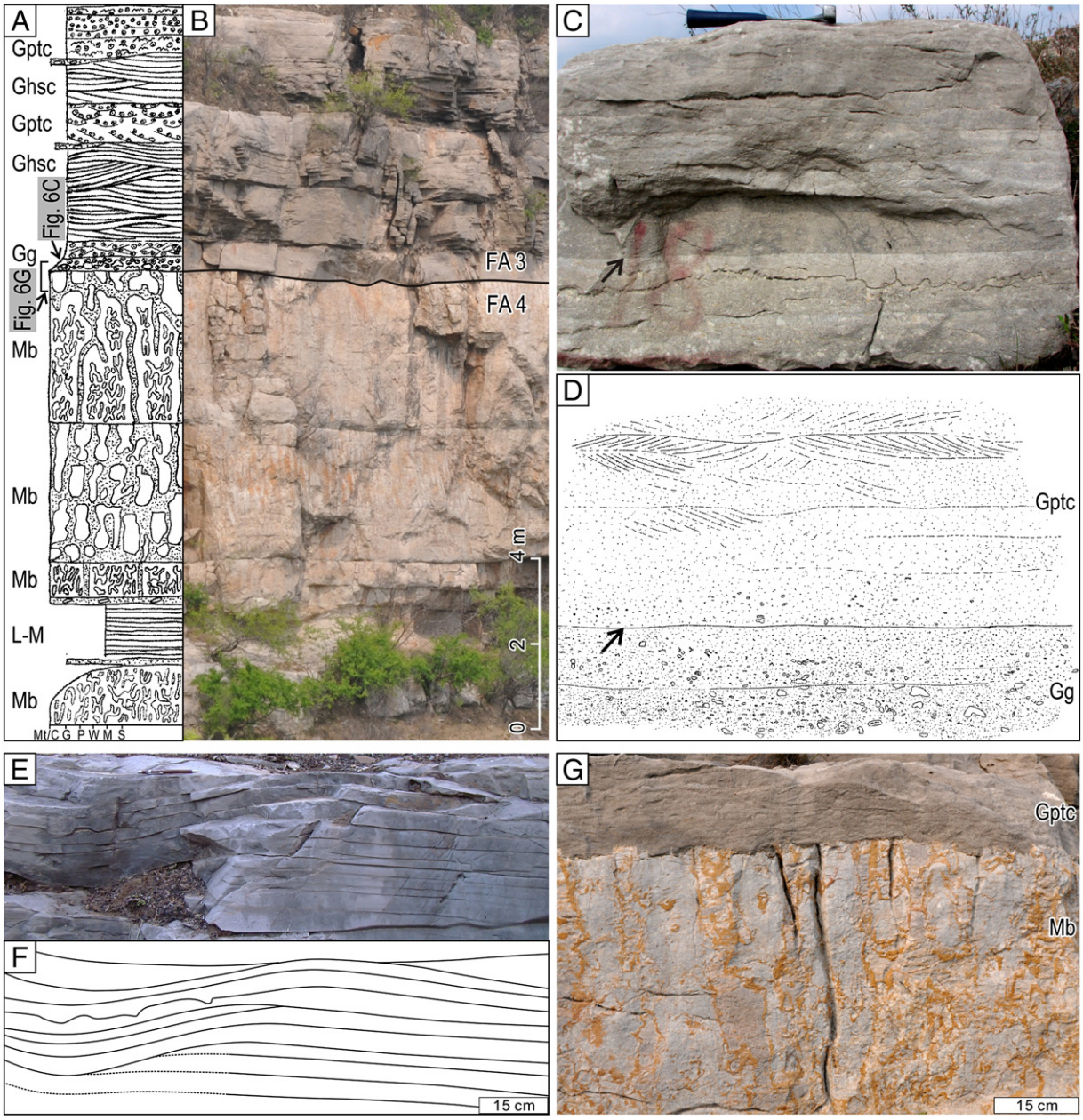

Fig. 6. Grainstone facies association (FA3) and microbialite facies association (FA4). A and B. A sedimentary log and photograph of FA3 and FA4 in the middle part of the Chaomidian Formation (Tangwangzhai section) (for location, see Fig. 3). S: shale, M: lime mudstone, W: wackestone, P: packstone, G: grainstone, C: limestone conglomerate, and Mt: microbialite. C and D. Gravelly grainstone, and planar and trough cross-stratified grainstone (facies Gg and Gptc) with a sharp internal boundary (arrows). Hammer for scale is 28 cm in length. E and F. Hummocky cross-stratified grainstone (facies Ghsc) (for location, see Fig. 3). G. Columnar microbialite (facies Mb), overlain by a planar cross-stratified grainstone (facies Gptc) with an irregular sharp boundary.

(Fig. 12B). The limestone breccia with totally disrupted clasts (inclined, vertical, and disorganized) occurs locally in the uppermost part of the deformed bed in the Wanliangyu section (Figs. 9 and 10).

Interpretation: The breccia with various positions of the clasts was formed by soft-sediment deformation of thin-bedded lime mudstones during early diagenesis (Chough et al., 2001; Kwon et al., 2002; Chen et al., 2009a). The bent and subrounded clasts indicate that the thin-bedded lime mud layers had not completely become consolidated or cemented during deformation, whereas the flat and angular clasts indicate that they were well consolidated. The (semi) consolidated and stiff thin lime mudstone deposits were most likely brecciated due to high cohesion and rigidity by mechanical rupture and/or injection of liquefied sediment (cf. Cowan and James, 1992; Spence and Tucker, 1997; Molina et al., 1998; Pratt, 1999). The clasts were subsequently dislocated and disrupted, forming flat pebble- to cobble-size clasts with various orientations (horizontal, inclined, vertical, and disorganized) (Chen et al., 2009a).

5.2.2. Chaotic wacke-packstone laminae and fragments

Description: The chaotic wacke-packstone laminae and fragments commonly co-occur in the deformed bed (Figs. 10 and 11). They are mainly composed of fossil fragments (e.g., trilobites, bivalves, and algae), glauconite grains, and a groundmass of lime mud (Fig. 12C, D). The chaotic laminae are largely convoluted and distorted. The laminae (up to 0.3 mm thick) are usually crude and irregular (Fig. 12E), and commonly occur around the fragments, among the brecciated thin limestone beds, or in the clastic dykes. The laminae are composed of either lime mudstone or bioclastic wackestone to packstone. The fossil fragments are commonly oriented following the bioclastic laminae

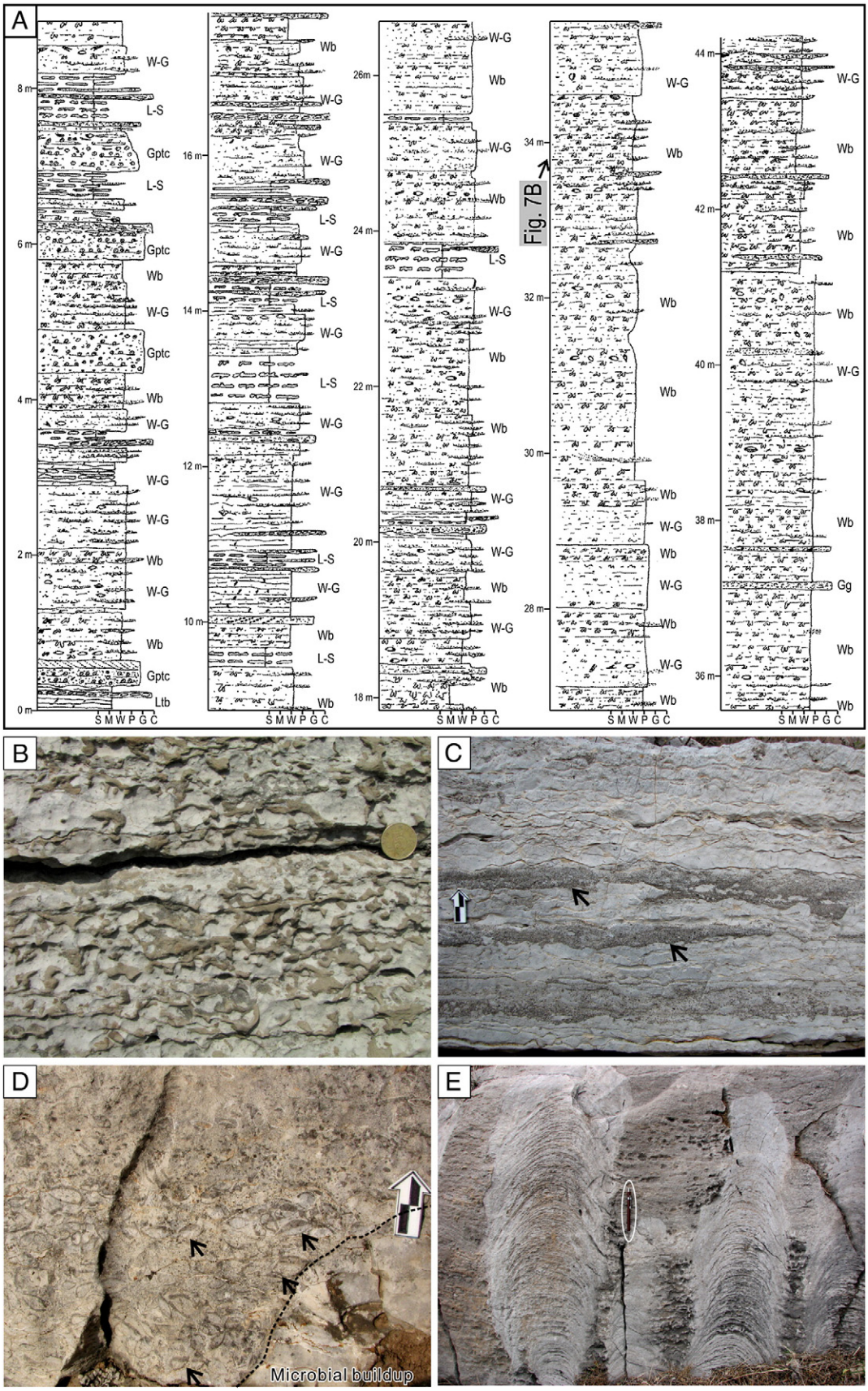

Fig. 7. Bioturbated wackestone to grainstone facies association (FA5). A. A sedimentary log of FA5 in the upper part of the Chaomidian Formation (Laopozhuang section). S: shale, M: lime mudstone, W: wackestone, P: packstone, G: grainstone, C: limestone conglomerate, and Mt: microbialite. L–S: limestone/shale alternation, Wb: bioturbated wackestone, W–G: wackestone to grainstone, Gptc: planar and trough cross-stratified grainstone, Gg: gravelly grainstone. B. Severely bioturbated wackestone (facies Wb). Coin for scale is 2 cm in diameter. C. Wackestone to grainstone (facies W–G) with sharp boundaries (arrows). Scale bar in C and D is 2 cm long. D. Rich concentration of bivalve shells with geopetal structures (arrows). E. Columnar stromatolite (facies Sc) with convex-up laminae. Pencil for scale is 14.2 cm in length. For figure locations, see Fig. 3.

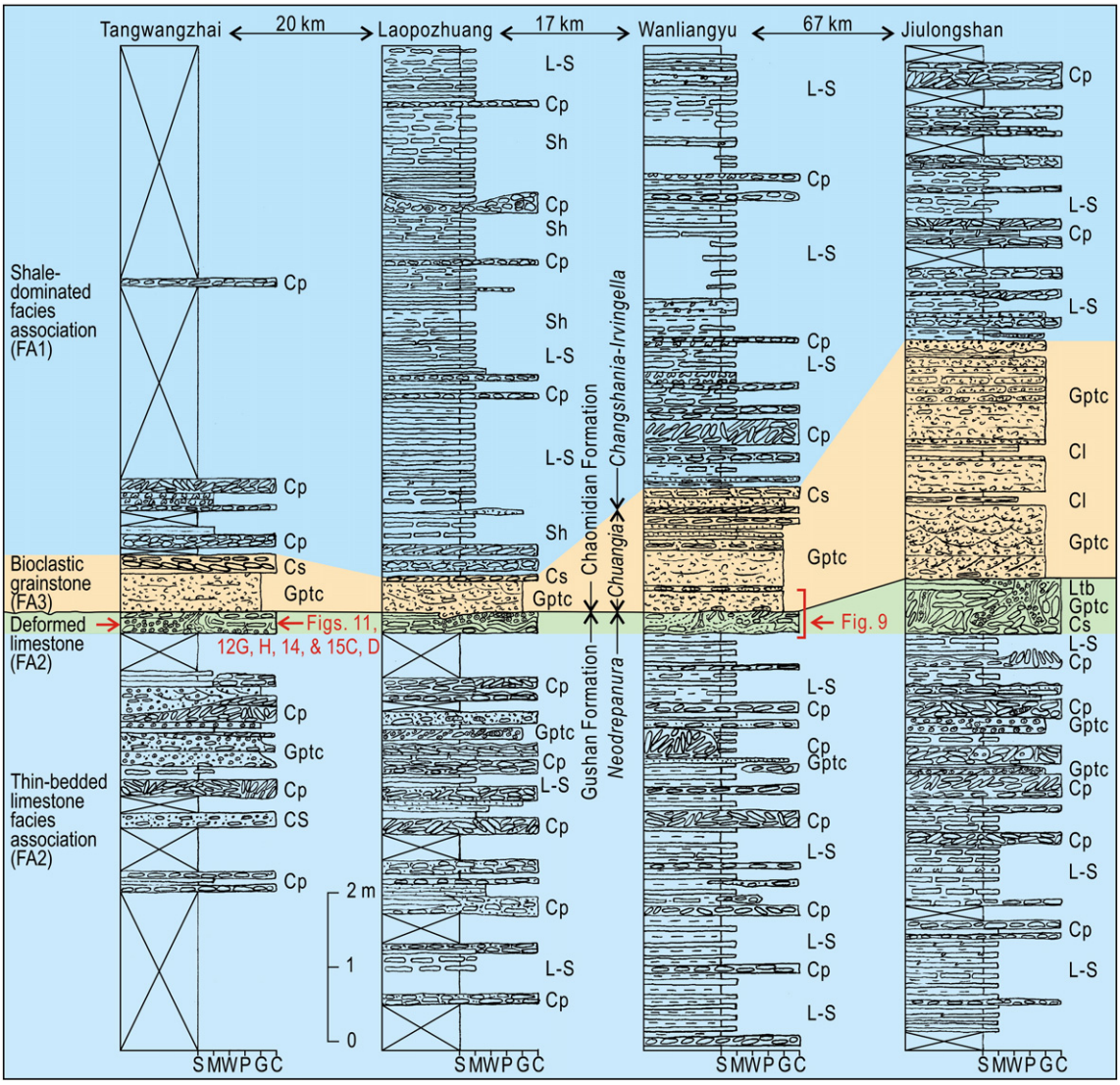

Fig. 8. Sedimentary logs of four major outcrop sections (for location, see Fig. 1B), showing correlation of the deformed limestone bed and the associated lithology. S: shale, M: lime mudstone, W: wackestone, P: packstone, G: grainstone, C: limestone conglomerate. Sh: shale, L–S: limestone/shale alternation, Cl: laminated calcisiltite, Gptc: planar and trough cross-stratified grainstone, Cs: stratified limestone conglomerate, and Cp: limestone breccia.

(Fig. 12C). The fragments vary in size (a few mm to a cm) and are largely equant in shape with slightly rounded corners (Fig. 12F).

Interpretation: It is not likely that the laminae were formed by deformation of original depositional laminae (i.e., convolute laminae) because convolute laminae are usually continuous and traceable (e.g., Nichols, 2009). Instead, these chaotic laminae seem to have been formed at the time of deformation. The mixture of bioclasts and lime mud was probably partly liquefied and/or fluidized; the unliquefied, relatively consolidated sediment became fragmented, whereas the partly liquefied sediment among the fragments was subject to hydroplastic deformation (cf. Pope et al., 1997; Onasch and Kahle, 2002). The laminae were formed by dewatering and flowage of the liquefied sediment under differential compaction (cf., Braccini et al., 2008; Scott et al., 2009).

5.2.3. Homogenized (massive) oolite

Description: The homogenized structures occur only in oolite (Fig. 12G). The undeformed oolite is usually planar and trough cross-stratified with undulatory bedforms. The homogenized oolite is largely massive, partly containing a few granule- to cobble-size clasts of lime mudstone and wacke-packstone fragments (Fig. 12G). The oolite is mainly composed of spheroidal ooids (partly broken) and a small portion of bioclasts, intraclasts, and glauconite grains; it has a sparite cement or micrite matrix (Fig. 12H). Oolite fragments with indistinct unit boundaries partly occur in the homogenized oolite. The homogenized (massive) oolite beds are commonly discontinuous and show discordant bed geometries. The homogenized oolites occasionally form clastic dykes, sharply cutting the laterally adjacent deposits (Fig. 12G).

Interpretation: Carbonate grains (consisting mostly of ooids, bioclasts, and peloids) became, if not completely cemented, either liquefied due to a high pore-water pressure or fluidized by upward injection of pore water (cf. Cowan and James, 1992). The liquefied/fluidized oolites thus were homogenized and formed structureless masses (cf. Pope et al., 1997; Onasch and Kahle, 2002). On the other hand, carbonate grains are easily cemented by early cementation (Cowan and James, 1992; Demicco and Hardie, 1994). The partially well-cemented, unliquefied oolites formed oolite fragments, which were incorporated in the liquefied material (cf., Chen et al., 2009b).

5.2.4. Clastic dykes

Description: The clastic dykes (a few mm to 10 cm in width, a few cm to tens of cm in thickness) are characterized by a discordant geometry, usually cutting through either the originally undeformed

Table 3
Soft-sediment deformation structures (SSDS) in the strongly deformed limestone bed.

SSDS and line drawings	Characteristics	Deformation processes
Lime mudstone breccias 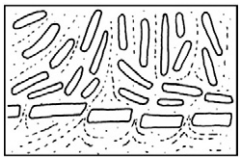	Monomictic to oligomictic pebble to cobble clasts of lime mudstone, with a matrix of oolite, marlstone, or bioclastic wackestone; clasts usually flat or bent disc and blade in shape with subrounded to angular corners; ample variation in position of clasts from horizontal and subhorizontal to inclined, vertical, and disorganized; progressive brecciation of thin limestone beds.	Brecciation and re-orientation of thin lime mudstone slabs by mechanical rupture and/or injection of liquefied sediment.
Wacke-packstone laminae and fragments 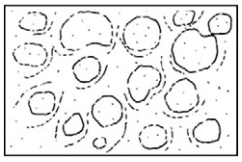	Chaotic laminae (up to 0.3 mm thick) and fragments commonly associated; composed of fossil fragments, glauconite grains, and lime mud; laminate either fine micritic (approx. 0.05 mm thick) or bioclastic with fossil fragments parallel to laminae; fragments from a few mm to a cm in size, largely equant in shape with slightly rounded corners and with diffuse and indistinct boundaries; random orientation.	Heterogeneous liquefaction/fluidization; laminae by dewatering and flowage of liquefied/fluidized sediment; fragments by unliquefied, relatively well-cemented bioclasts and lime mud.
Homogenized oolite 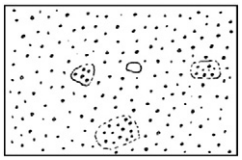	Occur commonly in oolites; homogenized oolites usually massive, composed of ooids (partly broken), bioclasts, and glauconite grains; partly containing a few granule to cobble clasts of lime mudstone and bioclastic wackestone fragments as well as oolite fragments with indistinct unit boundaries; discordant bed geometries, partly forming clastic dykes.	Liquefaction and/or fluidization of oolites; fragments formed by relatively well-cemented, unliquefied oolites.
Clastic dykes 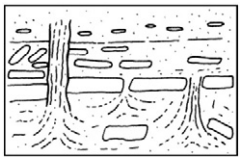	A few mm to 10 cm in width; a few cm to tens of cm in thickness; discordant geometry; consist of limestone breccias, massive oolites, or chaotic laminae of bioclastic wackestone; either vertical or inclined, upwards straight or variable in width; initiated from the base or the middle of the deformed deposits.	Upward escape and injection of liquefied and/or fluidized sediment due to the pressure of overburden.

deposits (e.g., stratified limestone conglomerates) or deformed deposits (e.g., lime mudstone breccias, and wacke-packstone laminae and fragments) (Figs. 10, 11, and 13). The clastic dykes consist mainly of lime mudstone breccias, homogenized oolites, or chaotic wacke-packstone laminae. The oolite dykes partly contain clasts of wacke-packstone laminae and fragments (Fig. 12G). They are either vertical

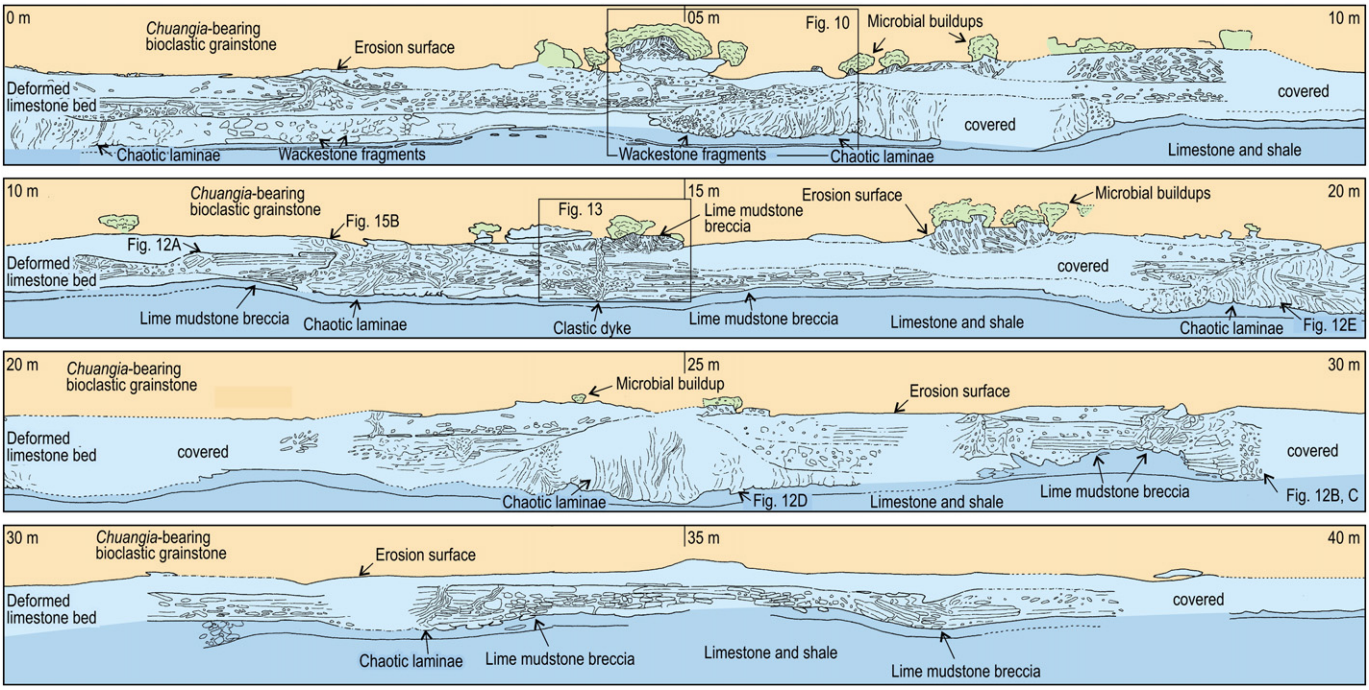

Fig. 9. Field sketch of the laterally continuous, strongly deformed limestone bed (containing a variety of deformation structures) in the Wanliangyu section (for location, see Figs. 1B and 8).

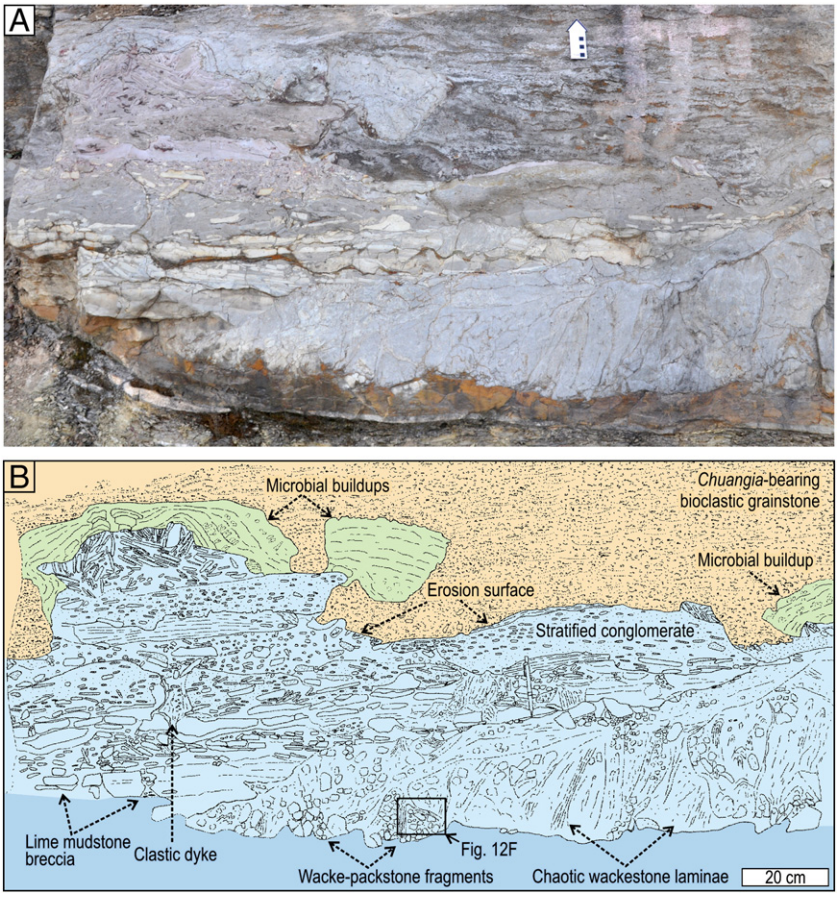

Fig. 10. Photograph (A) and line drawing (B) of the deformed limestone bed, overlain by a bioclastic grainstone bed with an irregular erosion surface (Wanliangyu section) (for location, see Fig. 9). Several small microbial buildups are present on the erosion surface. The deformed bed consists of several deformation structures such as lime mudstone breccias, clastic dykes, and chaotic wacke-packstone laminae and fragments.

or steeply inclined, and slightly variable in width. The clastic dykes were initiated from either the base or the middle part of the deformed interval (Figs. 10 and 13).

Interpretation: The clastic dykes were formed by upward injection of liquefied/fluidized sediment into the overlying deposits due to the pressure exerted by the overburden (Daley, 1971; Rossetti, 1999). They are not neptunian dykes or fills, because the constituent sediments in the dykes were originated from the lower-middle part of the deformed deposits, not from the overlying deposits (e.g., Desrochers and James, 1988; Smart et al., 1988; Wright, 1988). The upward escape of liquefied sediment resulted in various forms of clastic dykes. The incorporated clasts in the oolite dykes indicate that the oolite dykes were formed after the formation of other deformation structures such as lime mudstone breccias and wacke-packstone fragments.

5.3. Trigger mechanisms of deformation

The deformed limestone bed was most likely not related to karstification (subaerial solution-collapse) because both the bent clasts and the associated liquefaction and injection structures (i.e., chaotic laminae and fragments, homogenized oolites, and clastic

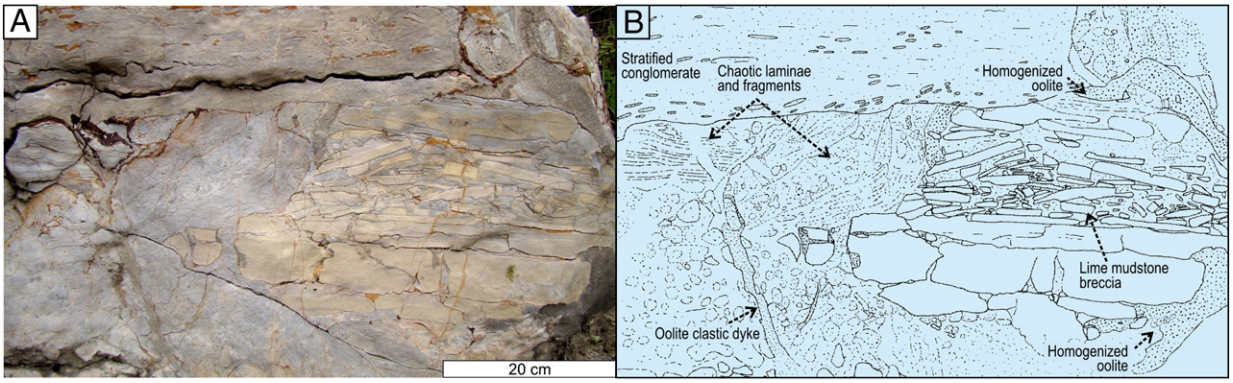

Fig. 11. Photograph (A) and line drawing (B) of the deformed limestone bed, containing several deformation structures such as lime mudstone breccias, chaotic wacke-packstone laminae and fragments, homogenized oolites, and clastic dykes (for location, see Fig. 8).

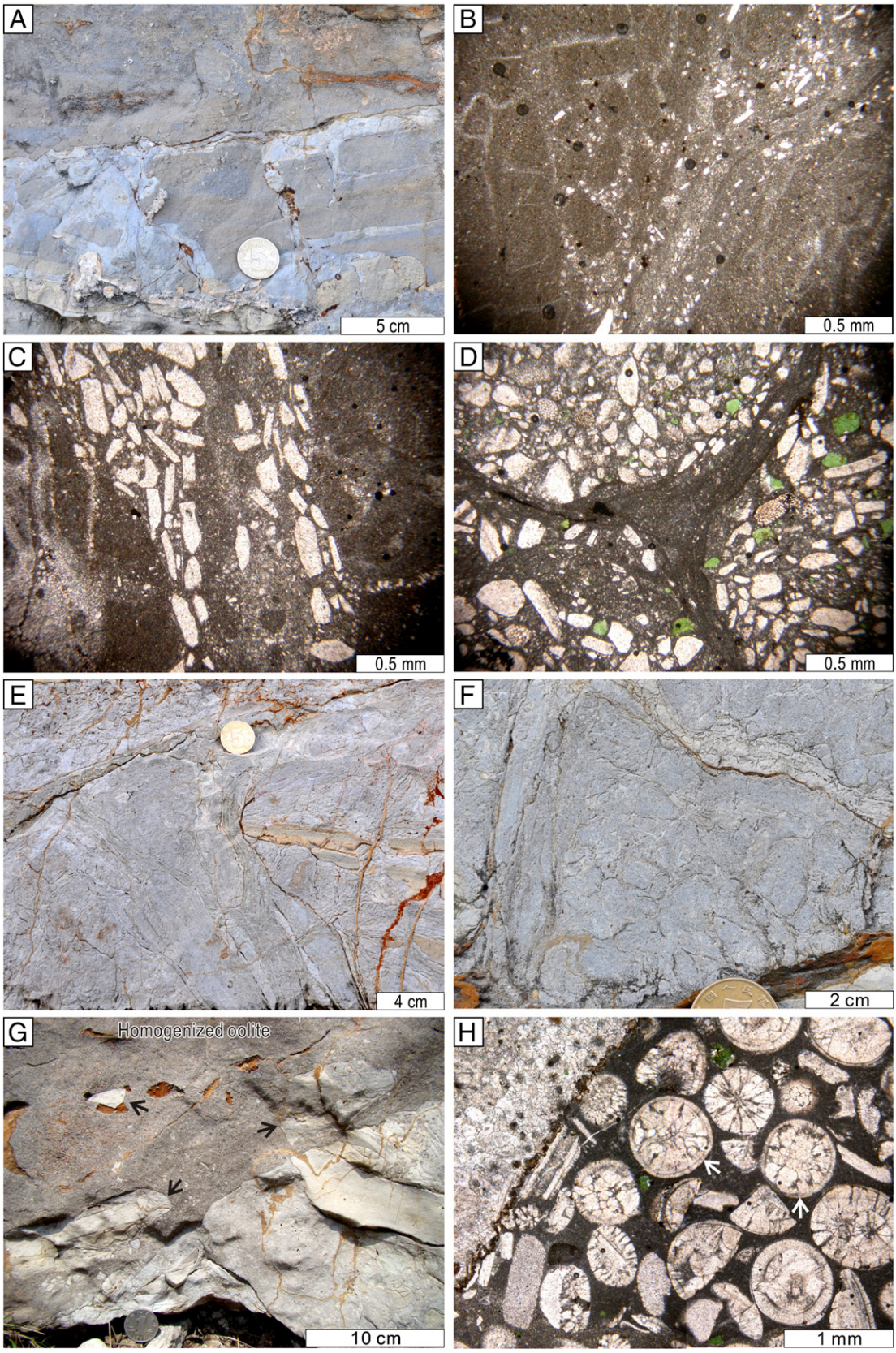

Fig. 12. Photographs and photomicrographs of the deformation structures. A. Photograph of a lime mudstone breccia with progressive brecciation of thin limestone bed. For locations of A–E, see Fig. 9. B. Photomicrograph of brecciated lime mudstone. Clasts on the left are *in situ* and angular, whereas those in the middle are displaced and slightly rounded. Note also crude micritic laminae in the middle-right part. C. Photomicrograph of bioclastic laminae with fossil fragments parallel to the laminae. D. Photomicrograph of three bioclastic wackestone fragments separated by micritic laminae. E. Photograph of chaotic laminae, showing horizontal, inclined, vertical, and irregular forms. F. Photograph of wacke-packstone fragments, showing random orientation and indistinct unit boundaries (for location, see Fig. 10B). G. Photograph of homogenized oolites with a few clasts of lime mudstone and wacke-packstone of laminae and fragments (arrows). For locations of G and H, see Fig. 8. H. Photomicrograph of homogenized oolite that is composed of ooids (partly broken), fossil fragments, and a few glauconite grains in micrite matrix. Note the thin isopachous cement around ooids (arrows).

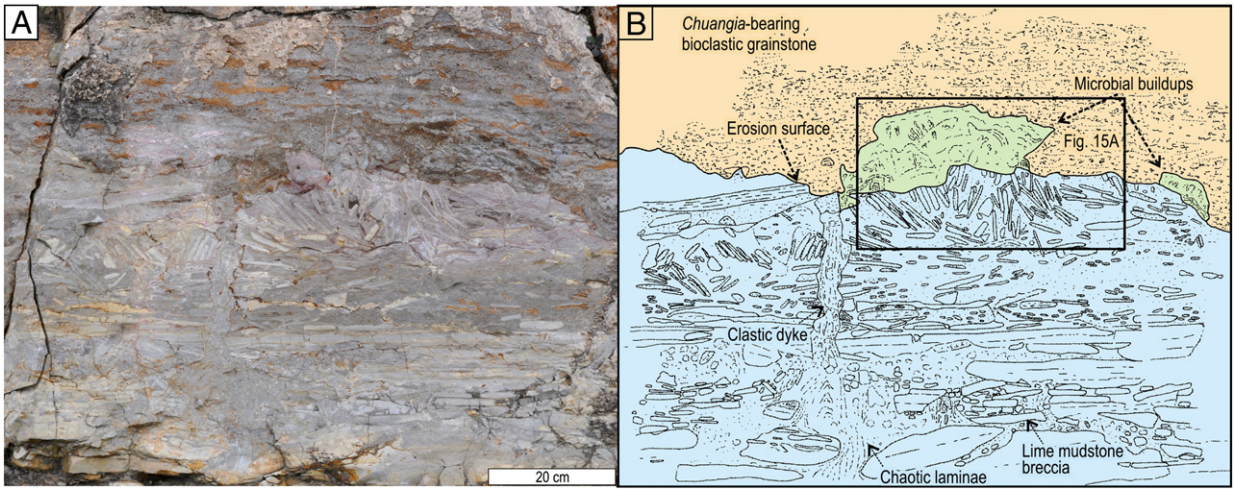

Fig. 13. Photograph (A) and line drawing (B) of a clastic dyke initiated from the base of the deformed bed. It is truncated by the erosion surface (for location, see Fig. 9).

dykes) are indicative of an unlithified state of sediments at the time of deformation (cf. De Voto, 1988; Onasch and Kahle, 2002). Instead, the deformation of the limestone beds might have taken place during early diagenesis (cf. Chen et al., 2009a). Deformation processes such as brecciation, liquefaction/fluidization, and injection commonly occur together during deformation, which results in a variety of complex deformation structures (Owen, 1987; Rossetti, 1999; Van Loon, 2009). A number of trigger mechanisms may induce soft-sediment deformation during early diagenesis, among which the most frequently discussed in literature are rapid sediment loading, slope failure, (storm) wave loading, seismic shocks, and sea-level fluctuations (Owen, 1996; Spence and Tucker, 1997; Kullberg et al., 2001; Alfaro et al., 2002; Moretti and Sabato, 2007; Singh and Jain, 2007; Chen et al., 2009a,b; Van Loon, 2009).

Rapid sedimentation on shallow carbonate platforms may occur during storms (Hardie, 1977; Wright, 1984; Wanless et al., 1988). The sediments deposited by a single storm event seem, however, too thin (5 mm to 2 cm in thickness) to trigger soft-sediment deformation in modern environments (Hardie, 1977; Wanless et al., 1988). On the other hand, there were no significant slopes on the North China epeiric platform which could trigger slope failure over a large area. Storm-wave-induced cyclic loading or rhythmic pounding of breaking waves (surges) can trigger soft-sediment deformation (Dalrymple, 1979; Molina et al., 1998; Chen et al., 2009a,b). Localized stress of storm-wave loading or pounding would not, however, synchronously affect such an extensive area. Earthquakes and sea-level fluctuations are the two mechanisms that may trigger extensive deformation, which might account for the formation of the deformed limestones.

Earthquakes generate stress in sediments, thus triggering soft-sediment deformation in active tectonic settings (Kullberg et al., 2001; Neuwerth et al., 2006; Singh and Jain, 2007; Gruszka and Van Loon, 2007). They can affect certain horizons of deformation over large areas (e.g., Sims, 1975; Van Loon, 2009). Earthquakes of over magnitude 5 (Moment Magnitude) can trigger liquefaction of unconsolidated sediments and form sills, dykes, and breccias, but only over a short distance (e.g., Wheeler, 2002; Gruszka and Van Loon, 2007). In order to trigger deformations in an extensive area (approx. 100 km), earthquakes of over magnitude 7 (Moment Magnitude) are necessary (Wheeler, 2002). The North China Platform was, however, tectonically stable during the late Middle Cambrian to Furongian (Meng et al., 1997). It is, therefore, unlikely that such a high-magnitude earthquake could have affected the North China Platform (cf. Mitrovica et al., 1996; Lykke-Andersen and Surlyk, 2004). Besides, no syndepositional faults that are closely associated with seismites (e.g., Onasch and Kahle, 2002) have been recognized in the late Middle Cambrian to Furongian succession.

Relative sea-level fluctuations can give rise to non-equilibrium changes between hydrostatic pressure in the water column and the pore-water pressure in fine-grained sediments (Hilbrecht, 1989). According to Hilbrecht's (1989) theoretical consideration and comparison with observations, about 10% of the hydrostatic pressure during a highstand in sea level is preserved as pore-water overpressure in sediments during sea-level fall. In carbonate systems, the pore-water pressure cannot easily dissipate through sediments because the permeability of carbonates is significantly lowered due to early cementation. The pore-water pressure may build up, and, if overcoming the shear strength of the sediments, may trigger sediment failure and deformation (Hilbrecht, 1989; Spence and Tucker, 1997). Poorly cemented carbonate particles (ooids, bioclasts, and peloids) may thus become liquefied, and will form various deformation structures such as chaotic laminae, homogenized masses, and dykes, whereas relatively well-cemented sediments will become fragmented. The upward injection and escape of the liquefied material may, in turn, fracture thin-bedded lime mud layers which are (semi) consolidated and stiff due to high cohesion and rigidity (Molina et al., 1998; Chen et al., 2009a).

6. Erosion surface of the deformed bed

6.1. Description of the erosion surface

The extensive erosion surface on the deformed limestone bed can be laterally traced over 100 km. The erosion surface truncates the underlying deposits with various deformation structures (e.g., lime mudstone breccias, chaotic wacke-packstone laminae and fragments, homogenized oolites, and clastic dykes) (Figs. 10, 13, 14, and 15). The deformed sediment often shows a thin isopachous cement (Fig. 12H), formed by early marine cementation. The meteoric cementation signatures (e.g., meniscus and “dripstone”-like cement due to meteoric vadose diagenesis and a drusy mosaic calcite cement due to meteoric phreatic diagenesis) are absent in the deformed sediment. The truncation surface is locally either planar or irregular with a relatively low relief (up to 20 cm in height) (Figs. 14 and 15). It is overlain by a *Chuangia*-bearing grainstones (0.6–4.5 m thick) that is composed mainly of fossil fragments (trilobites, brachiopods, and algae) with abundant glauconite grains. Glauconite grains are especially concentrated right above the erosion surface (Fig. 15C, D). The bioclastic grainstones are crudely planar to trough cross-stratified, and are, in turn, overlain by a shale-dominated facies association (FA1) (Fig. 8). Sporadic small-scale (cm to dm) microbial buildups that comprise mainly abundant lime mud and micritized microbial residues locally occur on the topographic highs of the

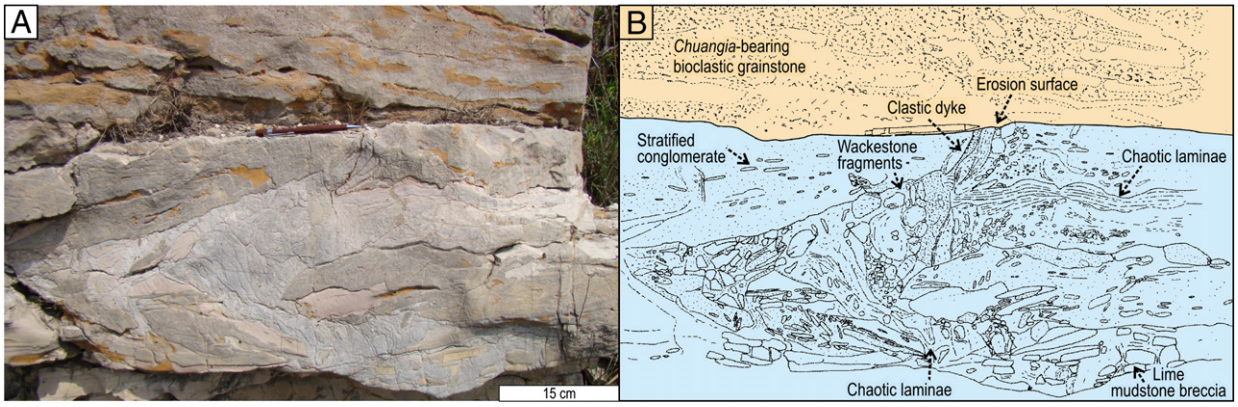

Fig. 14. Photograph (A) and line drawing (B) of the deformed limestone bed and the overlying bioclastic grainstones. Note the erosion surface that cuts the underlying deformed deposits with various deformation structures (for location, see Fig. 8).

erosion surface and under the extensive *Chuangia*-bearing grainstone (Fig. 9). The microbial buildups are also truncated, forming a sharp, irregular surface (Fig. 10).

The erosion surface is marked by the abrupt disappearance of the *Neodrepanura* biozone, the lack of the *Prochuangia* biozone, and the abrupt appearance of the *Chuangia* biozone (Figs. 2 and 8), which is also consistent with a worldwide mass extinction of trilobites (cf. Saltzman et al., 2000; Zhu et al., 2004). Newly acquired carbon isotope data across the erosion surface from the upper part of the Gushan Formation and the lower part of the Chaomidian Formation in the Wanliangyu section indicate that a positive excursion ($\delta^{13}C$ values up to +3.46‰) occurs above the surface (Table 4; Fig. 16). The positive excursion starts abruptly below the surface, reaches its peak in the *Chuangia*-bearing bioclastic grainstones, and ends gradually in the shale-dominated facies containing the *Changshania–Irvingella* biozone (Fig. 16). This positive excursion is well correlated among the early Furongian successions worldwide (e.g., Glumac and Walker, 1998; Saltzman et al., 2000, 2004; Zhu et al., 2004) (Fig. 16).

6.2. Formation of the erosion surface

The erosion surface of the deformed limestone bed indicates that erosion might have removed certain amounts of sediment because the deformed sediment was most likely buried at the time of deformation (cf. Hilbrecht, 1989; Chen et al., 2009a). According to Catuneanu et al. (2009), substantial sediment is removed by either subaerial or submarine erosion as a result of relative sea-level fall and rise, forming extensive erosion surfaces such as subaerial unconformities and transgressive ravinement surfaces, respectively. Submarine erosion (e.g., a transgressive ravinement) may scour and remove

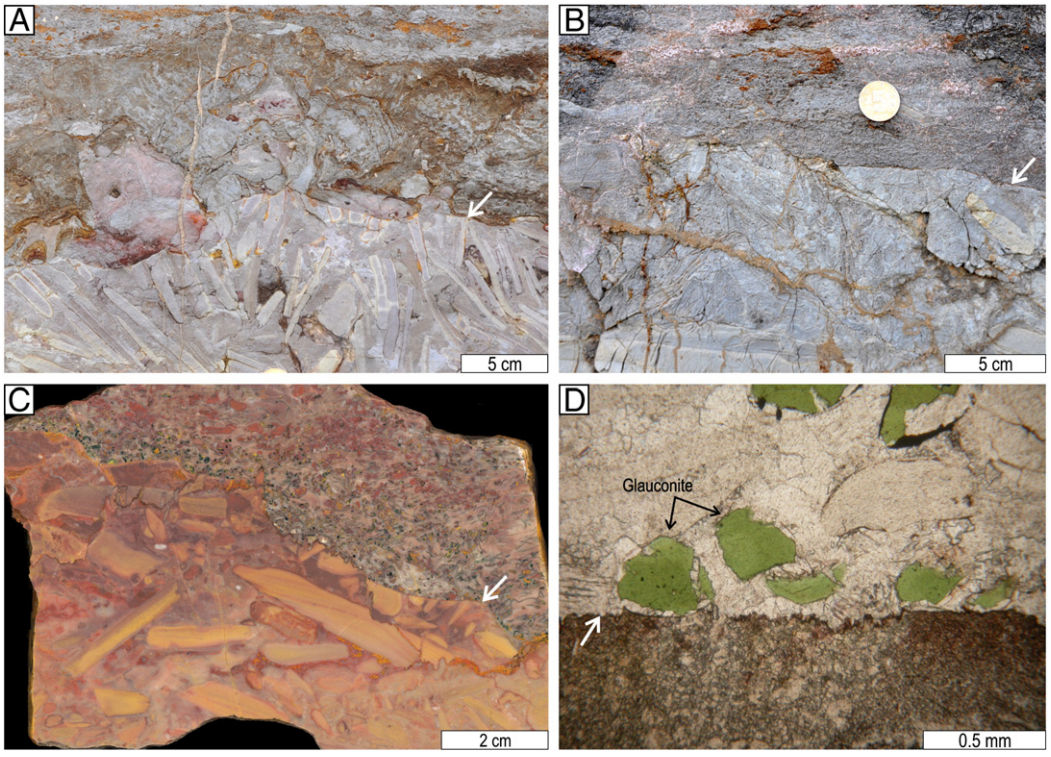

Fig. 15. Photographs of erosion surfaces (white arrows). A. Inclined and vertical clasts of a lime mudstone breccia were sharply cut and overlain by a microbial buildups (for location, see Fig. 13B). B. Chaotic laminae and wackestone fragments were sharply cut and overlain by the *Chuangia*-bearing bioclastic grainstone (for location, see Fig. 9). C. Polished slab. Both clasts and matrix of an originally deposited limestone conglomerate were sharply cut and overlain by the *Chuangia*-bearing bioclastic grainstone. For locations of C and D, see Fig. 8. D. Photomicrograph of a sharp contact between a clast of a limestone conglomerate below and bioclastic grainstone above. Note a rich concentration of glauconite grains above the erosion surface.

Table 4
Carbon isotope data from the upper part of the Gushan Formation and the lower part of the Chaomidian Formation in the Wanliangyu section (for location, see Fig. 1B).

Sample	$\delta^{13}C_{PDB}$	Lithology	No.	Sample	$\delta^{13}C_{PDB}$	Lithology	No.
C 30	0.506	Micrite	M10060	C 3	2.809	Micrite	M10033
C 29	0.634	Micrite	M10059	C 2	3.372	Micrite	M10032
C 28	0.675	Micrite	M10058	C + 1	3.223	Micrite	M10027
C 27	0.617	Micrite	M10057	C 1	3.352	Micrite	M10031
C 26	1.031	Micrite	M10056	C 0	2.809	Micrite	M10061
C 25	1.239	Micrite	M10055	G-2	1.414	Micrite	M10010
C 24	0.919	Micrite	M10054	G-1	0.145	Micrite	M10009
C 23	1.126	Micrite	M10053	G 0	0.599	Micrite	M10011
C 22	1.636	Micrite	M10052	G 1	0.493	Micrite	M10012
C 21	1.212	Micrite	M10051	G 2	0.864	Micrite	M10013
C 20	1.068	Micrite	M10050	G 3	0.891	Micrite	M10014
C 19	1.165	Micrite	M10049	G 4	0.448	Micrite	M10015
C 18	1.363	Micrite	M10048	G 5	0.531	Micrite	M10016
C 17	1.419	Micrite	M10047	G 6	0.223	Micrite	M10017
C 16	1.336	Micrite	M10046	G 7	0.550	Micrite	M10018
C 15	1.577	Micrite	M10045	G 8	0.658	Micrite	M10019
C 14	1.201	Micrite	M10044	G 9	0.757	Micrite	M10020
C 13	1.398	Micrite	M10043	G 10	0.420	Micrite	M10021
C 12	1.815	Micrite	M10042	G 11	0.253	Micrite	M10022
C 11	1.884	Micrite	M10041	G 12	0.198	Micrite	M10023
C 10	1.824	Micrite	M10040	G 13	0.243	Micrite	M10024
C 9	2.000	Micrite	M10039	G 14	0.347	Micrite	M10025
C 8	2.023	Micrite	M10038	G 15	0.149	Micrite	M10026
C 7	2.206	Micrite	M10037	G 17	0.194	Micrite	M10028
C 6	2.861	Micrite	M10036	G 18	0.087	Micrite	M10029
C 5	3.000	Micrite	M10035	G 19	0.163	Micrite	M10030
C 4	3.460	Micrite	M10034				

substrate soft sediment as a function of wave energy (Demarest and Kraft, 1987; Abbott, 1998; Catuneanu, 2006). It is, however, hard to imagine that submarine erosion is capable of removing thick interval of lithified sediment. Subaerial erosion may have played a role to form the erosion surface, although the subaerial exposure features (e.g., paleokarst, paleosols, and meteoric cementation signatures) are absent.

Evidence of subaerial exposure and erosion comes from the positive carbon isotope excursion (above the erosion surface), which can be correlated with those recognized in Laurentia and other continents (South China, Australia, and Kazakhstan) (Saltzman et al., 2000; Zhu et al., 2004). The positive excursion has been interpreted as a result of either increased isotope equilibrium exchange reactions within the inorganic carbon system by increased weathering of exposed carbonate platforms (cf. Kump et al., 1999) or increased percentage of the total carbon buried as organic matter in fine-grained siliciclastic deposits by increased weathering rate during exposure and erosion of carbonate platform interior (Saltzman et al., 2004). Either of the interpretations is suggestive of a subaerial exposure. The excursion in Laurentia is consistent with the Sauk II–III sequence boundary formed by a forced regression during the Steptoean Stage (coeval with the early Changshanian Stage in the North China Platform) (Glumac and Walker, 1998; Saltzman et al., 2004), which consequently provokes an argument for eustatic vs. relative sea-level fall during the end-Middle Cambrian (Saltzman et al., 2004). *Prochuangia* fauna was most likely pandemic in the entire North China Platform (cf. Alvaro et al., 2003; Peng, 2009). The missing of the *Prochuangia* biozone in Shandong Province, also manifested by an abrupt increase in carbon isotope values (Fig. 16), was most likely due to non-deposition under subaerial exposure conditions. It is a similar case to the local absence of the *Dunderbergia* biozone in the Steptoean succession in Laurentia (e.g., Wyoming and Vermont areas) (cf. Saltzman et al., 1998; Glumac and Spivak-Birndorf, 2002; Saltzman et al., 2004).

The exposed paleo-seafloor of the platform was most likely modified by subaerial weathering and erosion, but leaving scarce exposure features except for the sharp, irregular surface. The deformed sediment had been already fully cemented by contemporaneous marine cementation prior to the erosion, which resulted in the absence of vadose cementation (cf. Wright, 1982). Other exposure features such as paleokarst and paleosol did not develop, probably due to the unfavorable subaerial exposure conditions (e.g., short duration of exposure, relatively arid climate, or no vegetation or pedogenesis) (Holland and Patzkowsky, 1998). On the other hand, the sharp, irregular surface on the sporadic, small microbial buildups was formed by transgressive erosion during the subsequent sea-level rise, which indicates that the subaerial exposure surface might be also partly modified by submarine erosion (cf. Holland and Patzkowsky, 1998; Caron et al., 2004). The erosion surface might have been locally imprinted by pressure-dissolution during late diagenesis, and partly resembles karst-related dissolution features (i.e., lapiaz morphologies) (cf. Wright, 1982; George and Chow, 1999).

6.3. Submergence of the erosion surface

During the subsequent rise in sea level, the subaerial erosion surface was submerged. Sporadic microbial buildups preferentially developed on the topographic highs of the submerged erosion surface (hardground) (Parcell, 2002). The small-scale microbial buildups and the generally fine-grained character of the buildups are suggestive of deepened-water conditions. With the subsequent transgression, freshly deposited sediments (containing *Chuangia*) were constantly reworked by waves and currents, forming a lag deposit of shells (mainly trilobite and brachiopod) and glauconite grains during the phases of a low sedimentation rate (cf. Kidwell, 1989, 1991; Saltzman et al., 1995; Cattaneo and Steel, 2003). The *Chuangia*-bearing grainstone was successively overlain by an interval of shale-dominated facies (FA1) (Figs. 3 and 8), suggesting that the platform became submerged again with the ensued rise in sea level.

7. Discussion: sequence–stratigraphic implications

Sequence boundaries are bounding surfaces of relatively conformable successions, which are indicative of relative sea-level changes. They can be either subaerial unconformities and their correlative conformities (Vail et al., 1984) or maximum flooding surfaces (Galloway, 1989) and drowning unconformities (Schlager, 1999). It is essential to identify sequence boundaries in order to understand sequence development of the carbonate platforms. In the North China Platform of the Cambrian epeiric sea, sediments in the upper part of the Gushan Formation were deposited in a shallow-subtidal setting during sea-level highstand (HST) (Fig. 17A). Induced by a rapid fall in sea level, sediments were deformed by pore-water overpressure (Fig. 17B). The shallow-subtidal platform was consequently subaerially exposed as a result of the sea-level fall. The subaerial exposure resulted in the missing of the *Prochuangia* biozone and the excavation of the deformed sediment in the upper part of HST, forming an extensive erosion surface (Fig. 17C). During the subsequent rise in sea level, the subaerial erosion surface became submerged and a hardground surface formed with starved sedimentation, where sporadic small-scale microbial buildups developed (Fig. 17D). With continued transgression, freshly deposited sediments were winnowed and reworked by currents and waves in shoreface, forming a lag deposit (*Chuangia*-bearing grainstone) of the transgressive systems tract (TST) (Fig. 17E). The overlying deepening-upward, shale-dominated facies indicate submergence of the shoreface (Fig. 17F). Therefore, the erosion surface of the deformed limestone bed indicates a subtle sea-level change with a significant hiatus, forming a sequence boundary (Fig. 17G).

The late Middle Cambrian to Furongian succession (Gushan and Chaomidian formations) was previously subdivided into 2 third-order depositional sequences bounded by a marine flooding surface: the first one including the Gushan Formation and the lower part of the Chaomidian Formation; the second one including the upper part of the Chaomidian Formation (Meng et al., 1997). The erosion surface

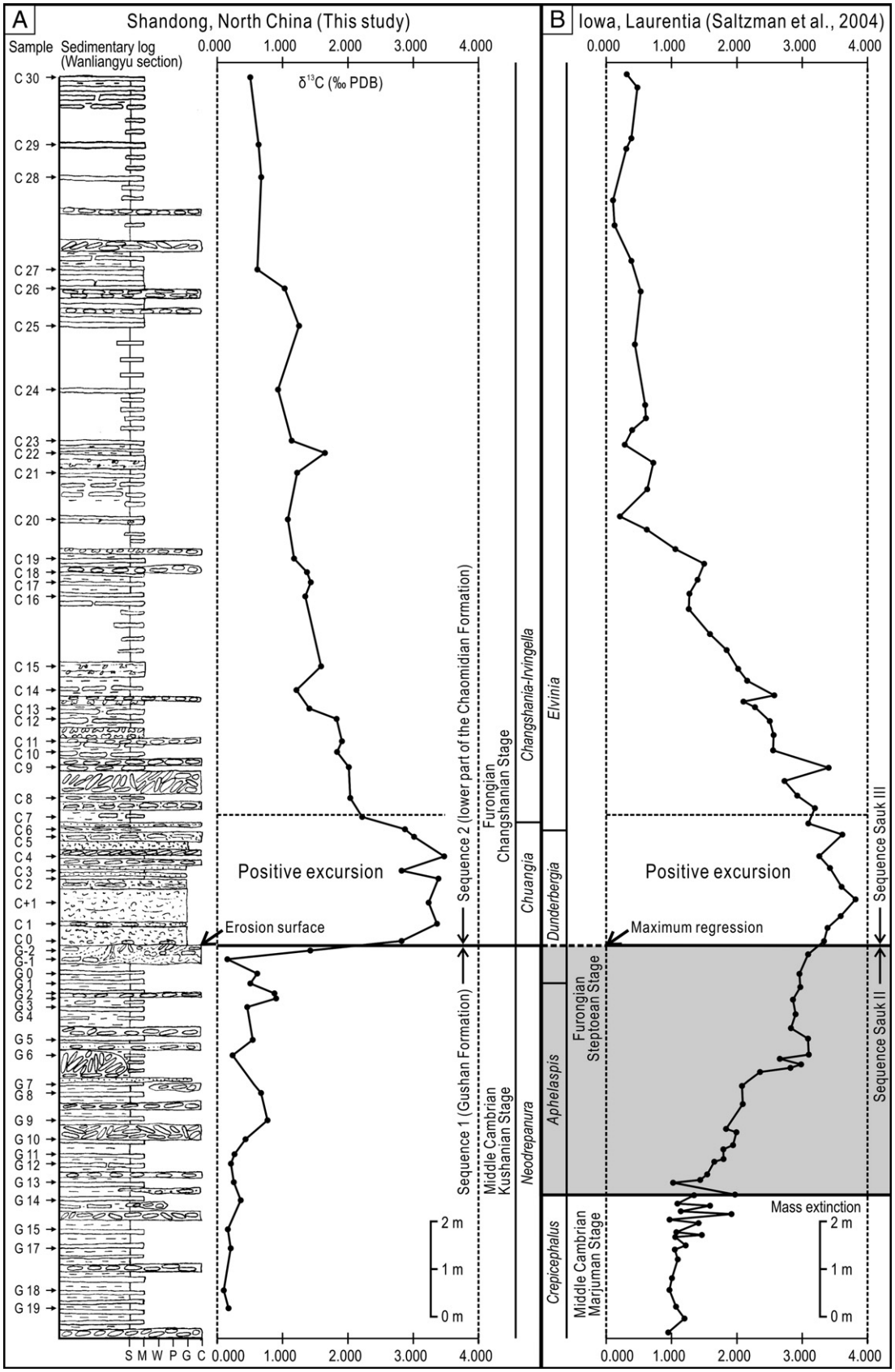

Fig. 16. A. Carbon isotope stratigraphy of the upper part of the Gushan Formation (late Middle Cambrian) and the lower part of the Chaomidian Formation (early Furongian) in the Wanliangyu section (for location, see Fig. 1B), showing a positive excursion ($\delta^{13}C$ values up to +3.46‰). The abrupt increase in $\delta^{13}C$ value across the erosion surface is probably due to missing of the *Prochuangia* biozone. S: shale, M: lime mudstone, W: wackestone, P: packstone, G: grainstone, and C: limestone conglomerate. B. Correlatable positive carbon isotope excursion in Laurentia (modified after Saltzman et al., 2004). Biostratigraphical correlation scheme is modified after Geyer and Shergold (2000) and Lee et al. (2008). The shaded zone is equivalent to the *Prochuangia* biozone that is missing in Shandong Province, China. The well-correlated positive carbon isotope excursion in the early Furongian may indicate a global regression (Saltzman et al., 2000, 2004).

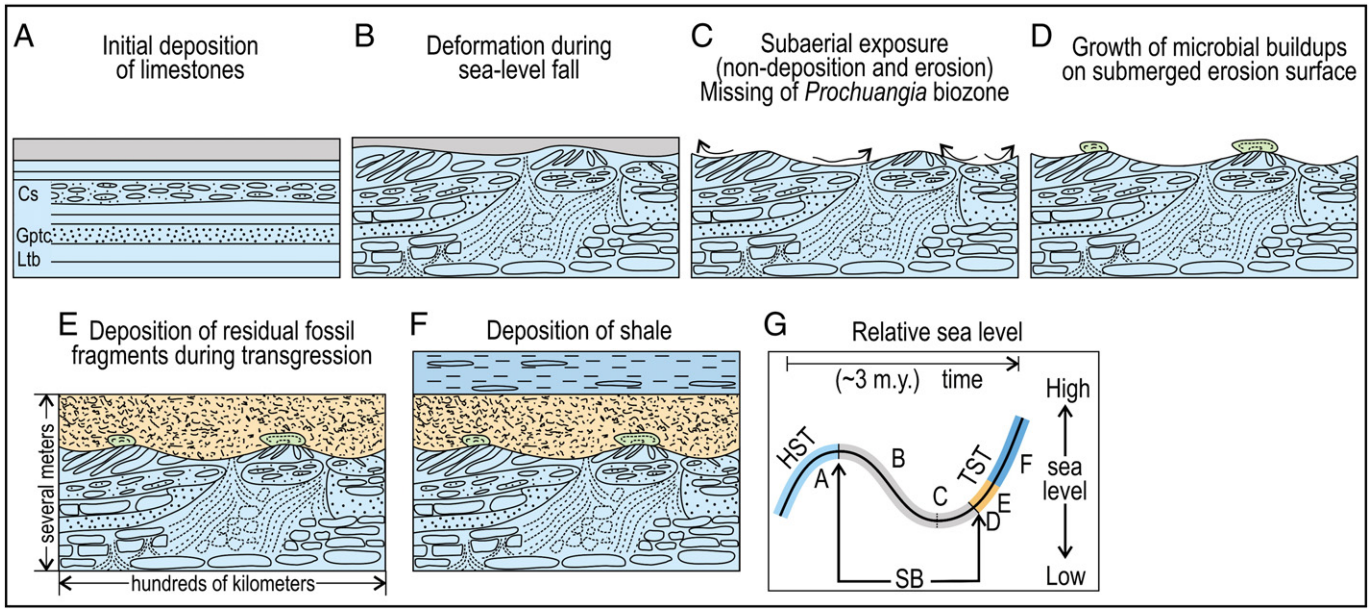

Fig. 17. A schematic model for the formation of the erosion surface and its sequence–stratigraphic implications. A. Deposition of thin-bedded lime mudstone (Ltb), stratified wackestone to grainstone (Gptc), and stratified limestone conglomerate (Cs) during a highstand in sea level (HST). B. Deformation of the limestone beds of HST during rapid sea-level fall. C. Non-deposition of the *Prochuangia* biozone and subaerial erosion during subaerial exposure due to the sea-level fall. D. Growth of microbial buildups on the submerged erosion surface during transgression (TST). E. Deposition of the *Chuangia*-bearing bioclastic grainstones by reworking of waves and/or currents with subsequent sea-level rise. F. Deposition of the shale-dominated facies during further rise in sea level. G. Relative sea-level curve, indicating stages of different sedimentary (erosional) responses. The unique erosion surface between HST and TST, accompanied with missing of a significant geological record, represents a (hidden) subaerial unconformity.

(subaerial unconformity) that separates the sequence 1 (Gushan Formation) below and sequence 2 (lower part of the Chaomidian Formation) above (Fig. 3) was apparently overlooked. Instead, Meng et al. (1997) interpreted the glauconite-rich interval (equivalent to the *Chuangia*-bearing grainstone above the erosion surface) as a maximum flooding zone of a second-order megasequence (Lower Cambrian through Lower Ordovician).

The shallow, relatively flat seafloor of the epeiric platforms can be completely or partly exposed subaerially as a result of high-order sea-level fluctuations (amplitudes approx. 20 ± 5 m) (cf. Osleger and Montañez, 1996). Sediments deposited during a sea-level highstand (HST) are expected to be reworked by subaerial weathering and erosion (e.g., karstification) during relative sea-level fall (Catuneanu et al., 2009), but subaerial exposure features do not necessarily develop, depending on the control factors such as duration of exposure, climate, vegetation, and pedogenesis (cf. Fouke et al, 1995; Holland and Patzkowsky, 1998; Budd et al., 2002). Besides, the subaerial exposure features can also be partly removed by submarine erosion during transgression (e.g., Caron et al., 2004). For these reasons, the subaerial erosion surfaces can be easily overlooked or mistaken as submarine erosion surfaces (cf. Holland and Patzkowsky, 1998; Caron et al., 2004). The unique relationship of the extensive deformed limestone bed and its erosion surface, combined with paleontological and geochemical data, may help distinguish the subaerial erosion surfaces from submarine erosion surfaces and identify the sequence boundary.

8. Conclusions

1. A strongly deformed limestone bed (containing *Neodrepanura*) with a variety of soft-sediment deformation structures occurs over an extensive area in the uppermost part of the Gushan Formation (late Middle Cambrian), Shandong Province, China. The extensive deformation most likely resulted from pore-water overpressure that was induced by a rapid fall in sea level.
2. The sea-level fall consequently caused subaerial exposure of the shallow North China epeiric platform, resulting in the missing of the *Prochuangia* biozone and formation of an extensive erosion surface on the deformed, contemporaneously well-lithified sediment. With the subsequent rise in sea level, the subaerial erosion surface was submerged, forming a submarine hardground on which sporadic microbial buildups locally developed. The *Chuangia*-bearing bioclastic grainstone (i.e., a transgressive lag deposit) formed on the shoreface with continued transgression, and the overlying shale-dominated facies indicates submergence of the shoreface.
3. The extensive erosion surface (i.e., a subaerial unconformity), combined with the missing of a geological record and the correlatable carbon isotope excursion, indicates a significant subaerial hiatus in the North China Platform during the late Middle Cambrian to Furongian. Detailed examination of the erosion surface of deformed limestone beds may help identify subtle (or hidden) third-order or higher-order deposition sequences in carbonate epeiric platforms.

Acknowledgements

The authors thank D.K. Choi, H.S. Lee, J. Woo, S.-b. Lee, and T.-Y. Park for useful discussions. The comments of A.J. van Loon and an anonymous reviewer greatly improved the earlier versions of the manuscript. This study was supported by grants to SKC by the National Research Foundation of Korea (2010-0029644) and the BK 21 project of Korea (Ministry of Education and Human Resources), and to ZH by the National Natural Science Foundation of China (40972043 and 41040018).

References

Abbott, S.T., 1998. Transgressive systems tracts and onlap shellbeds from Mid-Pleistocene sequences, Wanganui Basin, New Zealand. Journal of Sedimentary Research 68, 253–268.

Adams, R.D., Grotzinger, J.P., 1996. Lateral continuity of facies and parasequences in Middle Cambrian Platform Carbonates, Carrara Formation, Southeastern California, U.S.A. Journal of Sedimentary Research 66, 1079–1090.

Adams, E.W., Grotzinger, J.P., Watters, W.A., Schröder, S., McCormick, D.S., Al-Siyabi, H.A., 2005. Digital characterization of thrombolite–stromatolite reef distribution in a

carbonate ramp system (terminal Proterozoic, Nama Group, Namibia). AAPG Bulletin 89, 1293–1318.
Alfaro, P., Delgado, J., Estévez, A., Molina, J.M., Moretti, M., Soria, J.M., 2002. Liquefaction and fluidization structures in Messinian storm deposits (Bajo Segura Basin, Betic Cordillera, southern Spain). International Journal of Earth Science (Geol Rundsch) 91, 505–513.
Allen, P.A., 1985. Hummocky cross-stratification is not produced purely under progressive gravity waves. Nature 313, 562–564.
Alvaro, J.J., Elicki, O., Geyer, G., Rushton, A.W.A., Shergold, J.H., 2003. Palaeogeographical controls on the Cambrian trilobite immigration and evolutionary patterns reported in the western Gondwana margin. Palaeogeography, Palaeoclimatology, Palaeoecology 195, 5–35.
Arnott, R.W.C., Southard, J.B., 1990. Exploratory flow-duct experiments on combined-flow bed configurations, and some implications for interpreting storm-event stratification. Journal of Sedimentary Petrology 60, 211–219.
Betzler, C., Pawellek, T., Abdullah, M., Kossler, A., 2007. Facies and stratigraphic architecture of the Korallenoolith Formation in North Germany (Lauensteiner pass, Ith mountains). Sedimentary Geology 194, 61–75.
Braccini, E., de Boer, W., Hurst, A., Huuse, M., Vigorito, M., Templeton, G., 2008. Sand injectites. Oilfield Review 20, 34–49.
Budd, D.A., Gaswirth, S.B., Oliver, W.L., 2002. Quantification of macroscopic subaerial exposure features in carbonate rocks. Journal of Sedimentary Research 72, 917–928.
Burchette, T.P., Wright, V.P., 1992. Carbonate ramp depositional systems. Sedimentary Geology 79, 3–57.
Calvet, F., Tucker, M.E., 1988. Outer ramp cycles in the Upper Muschelkalk of the Catalan Basin, northeast Spain. Sedimentary Geology 57, 185–198.
Caron, V., Nelson, C.S., Kamp, P.J.J., 2004. Transgressive surfaces of erosion as sequence boundary markers in cool-water shelf carbonates. Sedimentary Geology 164, 179–189.
Cattaneo, A., Steel, R.J., 2003. Transgressive deposits: a review of their variability. Earth-Science Reviews 62, 187–228.
Catuneanu, O., 2006. Principles of sequence stratigraphy. Elsevier, Amsterdam. 375 pp.
Catuneanu, O., Abreu, V., Bhattacharya, J.P., Blum, M.D., Dalrymple, R.W., Eriksson, P.G., Fielding, C.R., Fisher, W.L., Galloway, W.E., Gibling, M.R., Giles, K.A., Holbrook, J.M., Jordan, R., Kendall, C.G., St, C., Macurda, B., Martinsen, O.J., Miall, A.D., Neal, J.E., Nummedal, D., Pomar, L., Posamentier, H.W., Pratt, B.R., Sarg, J.F., Shanley, K.W., Steel, R.J., Strasser, A., Tucker, M.E., Winker, C., 2009. Towards the standardization of sequence stratigraphy. Earth-Science Reviews 92, 1–33.
Chen, J.Y., Teichert, C., 1983. Cambrian cephalopods. Geology 11, 647–650.
Chen, J., Chough, S.K., Chun, S.S., Han, Z., 2009a. Limestone pseudoconglomerates in the Late Cambrian Gushan and Chaomidian Formations (Shandong Province, China): soft-sediment deformation induced by storm-wave loading. Sedimentology 56, 1174–1195.
Chen, J., Van Loon, A.J., Han, Z., Chough, S.K., 2009b. Funnel-shaped, breccia-filled clastic dykes in the Late Cambrian Chaomidian Formation (Shandong Province, China). Sedimentary Geology 221, 1–6.
Chough, S.K., Kwon, S.-K., Ree, J.-H., Choi, D.K., 2000. Tectonic and sedimentary evolution of the Korean peninsula: a review and new view. Earth-Science Reviews 52, 175–235.
Chough, S.K., Kwon, Y.K., Choi, D.K., Lee, D.J., 2001. Autoconglomeration of limestone. Geosciences Journal 5, 159–164.
Chough, S.K., Lee, H.S., Woo, J., Chen, J., Choi, D.K., Lee, S.-B., Kang, I., Park, T.-Y., Han, Z., 2010. Cambrian stratigraphy of the North China Platform: revisiting principal sections in Shandong Province, China. Geosciences Journal 14, 235–268.
Cowan, C.A., James, N.P., 1992. Diastasis cracks: mechanically generated synaeresis-like cracks in Upper Cambrian shallow water oolite and ribbon carbonates. Sedimentology 39, 1101–1118.
Daley, B., 1971. Diapiric and other deformational structures in an Oligocene argillaceous limestone. Sedimentary Geology 6, 29–51.
Dalrymple, R.W., 1979. Wave-induced liquefaction: a modern example from the Bay of Fundy. Sedimentology 26, 835–844.
Dalrymple, R.W., Narbonne, G.M., Smith, L., 1985. Eolian action and the distribution of Cambrian shales in North America. Geology 13, 607–610.
De Voto, R.H., 1988. In: James, N.P., Choquette, P.W. (Eds.), Late Mississippian Paleokarst and Related Mineral Deposits, Leadville Formation, Central Colorado. : Paleokarst. Springer, London, pp. 278–305.
Demarest II, J.M., Kraft, J.C., 1987. Stratigraphic record of Quaternary sea levels: implications for more ancient strata. In: Nummedal, D., Pilkey, O.H., Howard, J.D. (Eds.), Sea-Level Fluctuation and Coastal Evolution: SEPM Special Publication, 41, pp. 223–239. Tulsa, OK.
Demicco, R.V., Hardie, L.A., 1994. Sedimentary structures and early diagenetic features of shallow marine carbonates: SEPM Atlas Series 1, Tulsa, OK, p. 265.
Desrochers, A., James, N.P., 1988. Early Paleozoic surface and subsurface paleokarst: Middle Ordovician Carbonates, Mingan Islands, Quebec. In: James, N.P., Choquette, P.W. (Eds.), Paleokarst. Springer, London, pp. 183–210.
Dravis, J.J., 1983. Hardened subtidal stromatolites, Bahamas. Science 219, 385–386.
Driese, S.G., Sriniwasan, K., Mora, C.I., Stapor, F.W., 1994. Paleoweathering of Mississippian Monteagle Limestone preceding development of a lower Chesterian transgressive systems tract and sequence boundary, middle Tennessee and northern Alabama. GSA Bulletin 106, 866–878.
Drzewiecki, P.A., Simó, J.A., 2002. Depositional processes, triggering mechanisms and sediment composition of carbonate gravity flow deposits: examples from the Late Cretaceous of the south-central Pyrenees, Spain. Sedimentary Geology 146, 155–189.
Elrick, M., Snider, A.C., 2002. Deep-water stratigraphic cyclicity and carbonate mud mound development in the Middle Cambrian Marjum Formation, House Range, Utah, USA. Sedimentology 49, 1021–1047.
Fouke, B.W., Zwart, E.W., Everts, A.-J.W., Schlager, W., 1995. Carbonate platform stratal geometries and the question of subaerial exposures. Sedimentary Geology 97, 9–19.
Galloway, W.E., 1989. Genetic stratigraphic sequences in basin analysis. I. Architecture and genesis of flooding-surface bounded depositional units. AAPG Bulletin 73, 125–142.
Garrett, P., Smith, D.L., Wilson, A.O., Patriquin, D., 1970. Physiography, ecology and sediments of two Bermuda patch reefs. Journal of Geology 79, 647–668.
George, A.D., Chow, A.N., 1999. Palaeokarst development in a lower Frasnian (Devonian) platform succession, Canning Basin, northwestern Australia. Australian Journal of Earth Sciences 46, 905–913.
Geyer, G., Shergold, J.H., 2000. The quest for internationally recognized divisions of Cambrian time. Episodes 23, 188–195.
Glumac, B., Spivak-Birndorf, M.L., 2002. Stable isotopes of carbon as an invaluable stratigraphic tool: an example from the Cambrian of the northern Appalachians, USA. Geology 30, 563–566.
Glumac, B., Walker, K.R., 1998. A Late Cambrian positive carbon-isotope excursion in the southern Appalachians: relation to biostratigraphy, sequence stratigraphy, environments of deposition, and diagenesis. Journal of Sedimentary Research 68, 1212–1222.
Glumac, B., Walker, K.R., 2000. Carbonate deposition and sequence stratigraphy of the Terminal Cambrian Grand Cycle in the Southern Appalachians, U.S.A. Journal of Sedimentary Research 70, 952–963.
Grotzinger, J.P., 1986. Evolution of early Proterozoic passive-margin carbonate platform, Rocknest Formation, Wopmay Orgen, N.W.T., Canada. Journal of Sedimentary Petrology 56, 831–847.
Gruszka, B., Van Loon, A.J., 2007. Pleistocene glaciolacustrine breccias of seismic origin in an active graben (Central Poland). Sedimentary Geology 193, 93–104.
Hamon, Y., Merzeraud, G., 2008. Facies architecture and cyclicity in a mosaic carbonate platform: effects of fault-block tectonics (Lower Lias, Causses platform, south-east France). Sedimentology 55, 155–178.
Hardie, L.A., 1977. Sedimentation on the Modern Carbonate Tidal Flats of Northwest Andros Island, Bahamas. Baltimore, Maryland, The Johns Hopkins University Press. 202 pp.
Hilbrecht, H., 1989. Redeposition of Late Cretaceous pelagic sediments controlled by sea-level fluctuations. Geology 17, 1072–1075.
Holland, S.M., Patzkowsky, M.E., 1998. Sequence stratigraphy and relative sea-level history of the Middle and Upper Ordovician of the Nashville Dome, Tennessee. Journal of Sedimentary Research 68, 684–699.
James, N.P., Bourque, P.-A., 1992. Reefs and mounds. In: Walker, R.G., James, N.P. (Eds.), Facies models: response to sea level change: Geological Association of Canada, St. John's, Canada, pp. 323–348.
Keller, M., 1997. Evolution and sequence stratigraphy of an early Devonian carbonate ramp, Cantabrian Mountains, Northern Spain. Journal of Sedimentary Research 67, 638–652.
Kidwell, S.M., 1989. Stratigraphic condensation of marine transgressive records: origin of major shell deposits in the Miocene of Maryland. Journal of Geology 97, 1–24.
Kidwell, S.M., 1991. Taphonomic feedback (live/dead interactions) in the genesis of bioclastic beds: keys to reconstructing sedimentary dynamics. In: Einsele, G., Ricken, W., Seilacher, A. (Eds.), Cycles and Events in Stratigraphy. Springer, Berlin, pp. 268–282.
Kolata, D.R., Huff, W.D., Bergström, S.M., 2001. The Ordovician Sebree Trough: an oceanic passage to the Midcontinent United States. GSA Bulletin 113, 1067–1087.
Kullberg, J.C., Oloriz, F., Marques, B., Caetano, P.S., Rocha, R.B., 2001. Flat-pebble conglomerates: a local maker for Early Jurassic seismicity related to syn-rift tectonics in the Sesimbra area (Lusitanian Basin, Portugal). Sedimentary Geology 139, 49–70.
Kump, L.R., Arthur, M.A., Patzkowsky, M.E., Gibbs, M.T., Pinkus, D.S., Sheehan, P.M., 1999. A weathering hypothesis for glaciation at high atmospheric pCO_2 during the Late Ordovician. Palaeogeography, Palaeoclimatology, Palaeoecology 152, 173–187.
Kwon, Y.K., Chough, S.K., 2005. Sequence stratigraphy of the cyclic successions in the Dumugol Formation (Lower Ordovician), mideast Korea. Geosciences Journal 9, 305–324.
Kwon, Y.K., Chough, S.K., Choi, D.K., Lee, D.J., 2002. Origin of limestone conglomerates in the Choson Supergroup (Cambro–Ordovician), mid-east Korea. Sedimentary Geology 146, 265–283.
Kwon, Y.K., Chough, S.K., Choi, D.K., Lee, D.J., 2006. Sequence stratigraphy of the Taebaek Group (Cambrian–Ordovician), mideast Korea. Sedimentary Geology 192, 19–55.
Lee, S.-b., Lee, D.-C., Choi, D.K., 2008. Cambrian–Ordovician trilobite family Missisquoiidae Hupé, 1955: systematic revision and palaeogeographical considerations based on cladistic analysis. Palaeogeography, Palaeoclimatology, Palaeoecology 260, 315–341.
Lee, J.-H., Chen, J., Chough, S.K., 2010. Paleoenvironmental implications of an extensive maceriate microbialite bed in the Furongian Chaomidian Formation, Shandong Province, China. Palaeogeography, Palaeoclimatology, Palaeoecology 297, 621–632.
Lehrmann, D.J., Goldhammer, R.K., 1999. Secular variation in parasequence and facies stacking patterns of platform carbonates: a guide to application of stacking-pattern analysis in strata of diverse age and settings. In: Harris, P.M., Saller, A.H., Simo, T. (Eds.), Advances in Carbonate Sequence Stratigraphy: Application to Reservoirs, Outcrops and Models. : SEPM Special Publication, 63. SEPM, Tulsa, pp. 187–225.
Lykke-Andersen, H., Surlyk, F., 2004. The Cretaceous–Palaeogene boundary at Stevns Klint, Denmark: inversion tectonics or sea-floor topography? Journal of the Geological Society, London 161, 343–352.
Markello, J.R., Read, J.F., 1981. Carbonate ramp-to-deeper shale shelf transitions of an Upper Cambrian intrashelf basin, Nolichucky Formation, Southwest Virginia Appalachians. Sedimentology 28, 573–597.

Meng, X., Ge, M., Tucker, M.E., 1997. Sequence stratigraphy, sea-level changes and depositional systems in the Cambro-Ordovician of the North China carbonate platform. Sedimentary Geology 114, 189–222.
Meyerhoff, A.A., Kamen-Kaye, M., Chen, C., Taner, I., 1991. China — Stratigraphy, Paleogeography, and Tectonics. Kluwer Academic Publishers, Dordrecht, Netherlands. 188 pp.
Mitrovica, J.X., Pysklywec, R.N., Beaumont, C., Rutty, A., 1996. The Devonian to Permian sedimentation of the Russian Platform: an example of subduction-controlled long-wavelength tilting of continents. Journal of Geodynamics 22, 79–96.
Molgat, M., Arnott, R.W.C., 2001. Combined tide and wave influence on sedimentation patterns in the Upper Jurassic Swift Formation, south-eastern Alberta. Sedimentology 48, 1353–1369.
Molina, J.M., Alfaro, P., Moretti, M., Soria, J.M., 1998. Soft-sediment deformation structures induced by cyclic stress of storm waves in tempestites (Miocene, Guadalquivir Basin, Spain). Terra Nova 10, 145–150.
Moretti, M., Sabato, L., 2007. Recognition of trigger mechanisms for soft-sediment deformation in the Pleistocene lacustrine deposits of the Sant'Arcangelo Basin (Southern Italy): seismic shock vs. overloading. Sedimentary Geology 196, 31–45.
Moshier, S.O., 1986. Carbonate platform sedimentology, Upper Cambrian Richland Formation, Lebanon Valley, Pennsylvania. Journal of Sedimentary Petrology 56, 204–216.
Myrow, P.M., Southard, J.B., 1996. Tempestite deposition. Journal of Sedimentary Research 66, 875–887.
Myrow, P.M., Tice, L., Archuleta, B., Clark, B., Taylor, J.F., Ripperdan, R.L., 2004. Flat-pebble conglomerate: its multiple origins and relationship to metre-scale depositional cycles. Sedimentology 51, 973–996.
Nakazawa, T., Ueno, K., Kawahata, H., Fujikawa, M., Kashiwagi, K., 2009. Facies stacking patterns in high-frequency sequences influenced by long-term sea-level change on a Permian Panthalassan oceanic atoll: an example from the Akiyoshi Limestone, SW Japan. Sedimentary Geology 214, 35–48.
Neuwerth, R., Suter, F., Guzman, C.A., Gorin, G.E., 2006. Soft-sediment deformation in a tectonically active area: the Plio-Pleistocene Zarzal Formation in the Cauca Valley (Western Colombia). Sedimentary Geology 186, 67–88.
Nichols, G., 2009. Sedimentology and Stratigraphy (second edition). Wiley-Blackwell, Oxford, United Kingdom. 419 pp.
Onasch, C.M., Kahle, C.F., 2002. In: Ettensohn, F.R., Rast, N., Brett, C.E. (Eds.), Seismically induced soft-sediment deformation in some Silurian carbonates, eastern U.S. Midcontinent: Ancient Seismites, GSA special papers 359, Boulder, USA, pp. 165–176.
Osleger, D., Montañez, I.P., 1996. Cross-platform architecture of a sequence boundary in mixed siliciclastic-carbonate lithofacies, Middle Cambrian, southern Great Basin, USA. Sedimentology 43, 197–217.
Osleger, D., Read, J.F., 1991. Relation of eustasy to stacking patterns of meter-scale carbonate cycles, Late Cambrian, U.S.A. Journal of Sedimentary Petrology 61, 1225–1252.
Owen, G., 1987. Deformation processes in unconsolidated sands. In: Jones, M.E., Preston, R.M.F. (Eds.), Deformation of Sediments and Sedimentary Rocks. : Geological Society Special Publication, 29. Blackwell, pp. 11–24.
Owen, G., 1996. Experimental soft-sediment deformation: structures formed by liquefaction of unconsolidated sands and some ancient examples. Sedimentology 43, 279–293.
Palma, R.M., López-Gómez, J., Piethé, R.D., 2007. Oxfordian ramp system (La Manga Formation) in the Bardas Blancas area (Mendoza Province) Neuquén Basin, Argentina: facies and depositional sequences. Sedimentary Geology 195, 113–134.
Parcell, W.C., 2002. Sequence stratigraphic controls on the development of microbial fabrics and growth forms — implications for reservoir quality distributions in the Upper Jurassic (Oxfordian) Smackover Formation, Eastern Gulf Coast, USA. Carbonates and Evaporites 17, 166–181.
Park, T.-Y., Sohn, J.W., Lee, S.M., Choi, D.K., 2007. Lower Furongian silicified trilobite faunal assemblages from the Sesong Formation, Taebaek Group, Korea. In: Landing, E.D. (Ed.), Ediacaran–Ordovician of East Laurentia. : 12th international conference of the Cambrian Chronostratigraphy working group, S.W. Ford memorial volume, 510. New York State Museum Bulletin, pp. 88–89.
Payros, A., Pujalte, V., 2008. Calciclastic submarine fans: an integrated overview. Earth-Science Reviews 86, 203–246.
Peng, S.C., 2009. The newly-developed Cambrian biostratigraphic succession and chronostratigraphic scheme for South China. Chinese Science Bulletin 54, 4161–4170.
Pfeil, R.W., Read, J.F., 1980. Cambrian carbonate platform margin facies, Shady Dolomite, Southwestern Virginia, U.S.A. Journal of Sedimentary Petrology 50, 91–116.
Pope, M.C., Read, J.F., Bambach, R., Hofmann, H.J., 1997. Late Middle to Late Ordovician seismites of Kentucky, southwest Ohio and Virginia: sedimentary recorders of earthquakes in the Appalachian basin. GSA Bulletin 109, 489–503.
Pratt, B.R., 1999. Gas bubble and expansion crack origin of molar-tooth calcite structures in the Middle Proterozoic belt supergroup, Western Montana — discussion. Journal of Sedimentary Research 69, 1136–1140.
Rasmussen, K.A., Neumann, A.C., 1988. Holocene overprints of Pleistocene paleokarst: Bight of Abaco, Bahamas. In: James, N.P., Choquette, P.W. (Eds.), paleokarst. Springer, London, pp. 132–148.
Read, J.F., Goldhammer, R.K., 1988. Use of Fischer plots to define 3rd-order sea level curves in peritidal cyclic carbonates, Early Ordovician, Appalachians. Geology 16, 895–899.
Rees, E.I., Eagle, R.A., Walker, A.J.M., 1976. Trophic and Other Influences on Macrobenthos Population Fluctuations in Liverpool Bay. In: Persoone, G., Jaspers, E. (Eds.), Proceedings of the 10th European symposium on marine biology 2. Universa Press, Wetteren, Belgium, pp. 589–599.
Rossetti, D.D.F., 1999. Soft-sediment deformation structures in late Albian to Cenomanian deposits, São Luís Basin, northern Brazil: evidence for palaeoseismicity. Sedimentology 46, 1065–1081.
Saltzman, M.R., 1999. Upper Cambrian carbonate platform evolution, *Elvinia* and *Taenicephalus* zones (Pterocephaliid—Ptychaspid), Northwestern Wyoming. Journal of Sedimentary Research 69, 926–938.
Saltzman, M.R., Davidson, J.P., Holden, P., Runnegar, B., Lohmann, K.C., 1995. Sea-level-driven changes in ocean chemistry at an Upper Cambrian extinction horizon. Geology 23, 893–896.
Saltzman, M.R., Runnegar, B., Lohmann, K.C., 1998. Carbon isotope stratigraphy of Upper Cambrian (Steptoean Stage) sequences of the eastern Great Basin: record of a global oceanographic event. GSA Bulletin 110, 285–297.
Saltzman, M.R., Ripperdan, R.L., Brasier, M.D., Lohman, K.C., Robison, R.A., Chang, W.T., Peng, S.C., Ergaliev, G.K., Runnegar, B., 2000. A global carbon isotope excursion (SPICE) during the Late Cambrian: relation to trilobite extinctions, organic-matter burial and sea level. Palaeogeography, Palaeoclimatology, Palaeoecology 162, 211–223.
Saltzman, M.R., Cowan, C.A., Runkel, A.C., Runnegar, B., Stewart, M.C., Palmer, A.R., 2004. The Late Cambrian SPICE ($\delta^{13}C$) event and the Sauk II–Sauk III regression: new evidence from Laurentian Basins in Utah, Iowa, and Newfoundland. Journal of Sedimentary Research 74, 366–377.
Sanders, D., Höfling, R., 2000. Carbonate deposition in mixed siliciclastic–carbonate environments on top of an orogenic wedge (Late Cretaceous, Northern Calcareous Alps, Austria). Sedimentary Geology 137, 127–146.
Schlager, W., 1999. Type 3 sequence boundaries. In: Harris, P.M., Saller, A.H., Simo, T. (Eds.), Advances in Carbonate Sequence Stratigraphy: SEPM Special Publication, 63, pp. 35–45. Tulsa.
Scotese, C.R., McKerrow, W.S., 1990. Revised world maps and introduction. In: McKerrow, W.S., Scotese, C.R. (Eds.), Palaeozoic Palaeogeography and Biogeography: Geological Society Memoir, 12, pp. 1–21.
Scott, A., Vigorito, M., Hurst, A., 2009. The process of sand injection: internal structures and relationships with host strata (Yellowbank Creek Injectite Complex, California, U.S.A.). Journal of Sedimentary Research 79, 568–583.
Sims, J.D., 1975. Determining earthquake recurrence intervals from deformation structures in young lacustrine sediments. Tectonophysics 29, 144–152.
Singh, S., Jain, A.K., 2007. Liquefaction and fluidization of lacustrine deposits from Lahaul–Spiti and Ladakh Himalaya: geological evidences of paleoseismicity along active fault zone. Sedimentary Geology 196, 47–57.
Smart, P.L., Palmer, R.J., Whitaker, F., Wright, V.P., 1988. Neptunian dikes and fissure fills: an overview and account of some modern examples. In: James, N.P., Choquette, P.W. (Eds.), Paleokarst. Springer, London, pp. 149–166.
Spence, G.H., Tucker, M.E., 1997. Genesis of limestone megabreccias and their significance in carbonate sequence stratigraphic models: a review. Sedimentary Geology 112, 163–193.
Srinivasan, K., Walker, K.R., 1993. Sequence stratigraphy of an intrashelf basin carbonate ramp to rimmed platform transition: Maryville Limestone (Middle Cambrian), southern Appalachians. GSA Bulletin 105, 883–896.
Strasser, A., 1986. Ooids in Purbeck limestone (lowermost Cretaceous) of the Swiss and French Jura. Sedimentology 33, 711–727.
Tucker, M.E., Wright, V.P., 1990. Carbonate Sedimentology. Blackwell, Oxford. 482 pp.
Vail, P.R., Hardenbol, J., Todd, R.G., 1984. Jurrassic unconformities, chronostratigraphy and sea-level changes from seismic stratigraphy and biostratigraphy. In: Schlee, J.S. (Ed.), Interregional Unconformities and Hydrocarbon Accumulation: AAPG Memoir, 36, pp. 129–144.
Van Loon, A.J., 2009. Soft-sediment deformation structures in siliciclastic sediments: an overview. Geologos 15, 3–55.
Vanstone, S.D., 1998. Late Dinantian palaeokarst of England and Wales: implication for exposure surface development. Sedimentology 45, 19–38.
Walker, R.G., Plint, A., 1992. Wave- and storm-dominated shallow marine systems. In: Walker, R.G., James, N.P. (Eds.), Facies Models: Response to Sea Level Change. Geological Association of Canada, Newfoundland, pp. 219–238.
Wanless, H.R., Tyrrell, K.M., Tedesco, L.P., Dravis, J.J., 1988. Tidal flat sedimentation from Hurricane Kate, Caicos Platform, British West Indies. Journal of Sedimentary Petrology 58, 724–738.
Wheeler, R.L., 2002. Distinguishing seismic from nonseismic soft-sediment structures: criteria from seismic-hazard analysis. In: Ettensohn, F.R., Rast, N., Brett, C.E. (Eds.), Ancient Seismites: GSA special papers 359, Boulder, USA, pp. 165–176.
Woo, K.S., 1999. Cyclic tidal successions of the Middle Ordovician Maggol Formation in the Taebaeg area, Kangwondo, Korea. Geosciences Journal 3, 123–140.
Woo, J., 2009. The Middle Cambrian Zhangxia Formation, Shandong Province, China: depositional environments and microbial sedimentation. Ph.D. Thesis, Seoul National University, Seoul, South Korea.
Woo, J., Chough, S.K., 2007. Depositional processes and sequence stratigraphy of the Jigunsan Formation (Middle Ordovician), Taebaeksan Basin, mideast Korea: implications for basin geometry and sequence development. Geosciences Journal 11, 331–355.
Wright, V.P., 1982. The recognition and interpretation of paleokarsts: two examples from the Lower Carboniferous of South Wales. Journal of Sedimentary Petrology 52, 83–94.
Wright, V.P., 1984. Peritidal carbonate facies models: a review. Geological Journal 19, 309–325.
Wright, V.P., 1988. Paleokarsts and paleosols as indicators of paleoclimate and porosity evolution: a case study from the Carboniferous of South Wales. In: James, N.P., Choquette, P.W. (Eds.), Paleokarst. Springer, London, pp. 329–341.
Wright, V.P., 1994. Paleosols in shallow marine carbonate sequences. Earth-Science Reviews 35, 367–395.
Zhu, M.-Y., Zhang, J.-M., Li, G.-X., Yang, A.-H., 2004. Evolution of C isotopes in the Cambrian of China: implications for Cambrian subdivision and trilobite mass extinctions. Geobios 37, 287–301.